SLAC-PUB-5827
GSI-92-35
May 1992
(T/E)

Systematics of Charm Production in Hadronic Collisions

R. Vogt

Gesellschaft für Schwerionenforschung (GSI)
D-W-6100 Darmstadt, Germany

S. J. Brodsky*

Stanford Linear Accelerator Center
Stanford University
Stanford, California 94309

P. Hoyer

Department of Physics
University of Helsinki
SF–00170 Helsinki, Finland

We present a comprehensive QCD–based model for the x_f, p_T, and nuclear target dependence of open charm production in hadron–induced collisions. The predicted dependence on x_f and p_T reflects both leading–twist QCD fusion subprocesses, including shadowing and coalescence effects, and higher–twist intrinsic heavy–quark components of the hadron wavefunction. The model is compared with the systematics of charmed hadron production in $\pi^- p$, pp, $\pi^- A$, and pA collisions. We find that the data cannot be described by leading–twist QCD contributions alone. Several features of the data show the presence of higher–twist mechanisms of the type we consider. Differences in kinematic acceptance between various experiments may explain some of the apparent discrepancies in the available data.

(Submitted to Nuclear Physics B)

[0]*Supported by the U. S. Department of Energy under Contract No. DE-AC03-76SF00515.

Introduction

One of the most interesting, but complex, testing grounds of quantum chromodynamics is charm production in hadron and nuclear collisions. Although the 'fusion' reactions $gg \to Q\overline{Q}$ and $q\overline{q} \to Q\overline{Q}$ are expected to be the dominant subprocesses for heavy–quark Q production in QCD, some of the data for both hidden and open charm production are in striking conflict with predictions based on the leading power–law fusion reactions and QCD factorization. As we shall discuss here, the inadequacy of the QCD fusion model to account for important features of heavy–quark hadroproduction, including the excess production at high x_f, the dependence of charmonium production on the nuclear target, and the observed correlations of leading charmed hadrons with the projectile quantum numbers strongly suggests the presence of another $c\bar{c}$ production mechanism which becomes significant at large momentum fractions x_f and low transverse momentum p_T. In fact, as shown in Ref. [1], factorization–breaking QCD contributions to the cross section which are normally suppressed by powers of the quark pair mass, $M_{Q\overline{Q}}$, can become dominant at large x_f in the kinematic region where $(1-x_f)M^2_{Q\overline{Q}}$ is finite.

The cornerstone of most predictions involving hard inclusive reactions in high–energy physics is the factorization theorem [2] of perturbative QCD, separating the perturbatively calculable hard scattering quark and gluon dynamics from the nonperturbative bound state dynamics contained in the process–independent structure functions, $G_{a/A}(x,Q^2)$, and the jet fragmentation functions, $D_{H/c}(z,Q^2)$. For example, at high energies and to leading order in $1/M^2_{Q\overline{Q}}$, the inclusive production cross section of heavy quark pairs with invariant mass $M_{Q\overline{Q}}$ has the form

$$\frac{d\sigma_{AB\to Q\overline{Q}X}}{dx_a dx_b} = \sum_{ab} G_{a/A}(x_a, M^2_{Q\overline{Q}}) G_{b/B}(x_b, M^2_{Q\overline{Q}}) \hat{\sigma}_{ab\to Q\overline{Q}}(M^2_{Q\overline{Q}} = x_a x_b s, \alpha_s(M^2_{Q\overline{Q}})) \ . \quad (1)$$

This factorization holds for all projectiles and targets A and B: leptons, photons, hadrons, and nuclei. Here x is the boost–invariant light–cone momentum fraction of the interacting partons, $x_a = k_a^+/p_A^+ = (k_a^0 + k_a^z)/(p_A^0 + p_A^z)$. The momentum fraction of the pair is $x_f = x_a - x_b$. The factorization of the Drell–Yan process, $AB \to \mu^+\mu^- X$, has been proven to leading order in $1/Q^2$ by Bodwin and by Collins, Soper, and Sterman. The proof was then extended to next–to–leading twist by Qiu and Sterman [2]. Using factorization, the charmed quark fragmentation function $D_{H/c}(z,Q^2)$ can be obtained from $e^+e^- \to c\bar{c} \to HX$ data.

Although the magnitude of the inclusive charm cross section can be roughly understood on the basis of the fusion process including a K factor of order 3 from higher–order corrections the shape predicted for $d\sigma/dx_f(\pi N \to DX)$ [3] falls off much too rapidly in x_f if one uses conventional parameterizations of the quark and gluon structure functions and the $D_{H/c}(z,Q^2)$ measured in e^+e^- annihilation. Taken literally, QCD factorization applied to open charm hadroproduction also predicts strict independence of heavy–quark fragmentation from the production process. Thus no flavor correlations should exist between final–state charmed hadrons and the incident hadrons. However, several experiments have reported flavor correlations in charm production. A particularly

prominent effect was seen by the LEBC–EHS bubble chamber experiment in $\pi^- p$ interactions at 360 GeV [4]. The $D^-(\bar{c}d)$ and $D^0(c\bar{u})$, containing valence $\bar{u}$ and d quarks of the π^- projectile, dominate over nonleading $D^+(c\bar{d})$ and $\overline{D}^0(\bar{c}u)$ at large x_f. If the x_f dependence of the production cross section is parameterized as $(1-x_f)^n$, the data indicate $n = 1.8 \pm 0.6$ for leading D mesons and $n = 7.9 \pm 1.5$ for nonleading D production. A smaller, but still significant, leading charm effect was reported by the ACCMOR Collaboration [5] from charm production on a nuclear target, $\pi^-\mathrm{Cu} \to D^{\pm}X$ at 230 GeV/c. Using the above parameterization, they found $n = 3.23 \pm 0.29$ for leading D production and $n = 4.34 \pm 0.35$ for nonleading D's.

Leading charm production suggests a mechanism by which projectile spectators produced at small transverse momentum coalesce with charmed quarks to form the observed charmed hadrons [6,7]. In the case of proton projectiles, this effect should be particularly important in charmed baryon production. If factorization were strictly valid, the relative rate of Λ_c baryon and D meson production should be the same in e^+e^-, $\pi^- p$, and pp interactions. According to the ACCMOR data [8] on $\pi^-\mathrm{Cu}$ collisions, the $\Lambda_c/\overline{\Lambda}_c$ and $D/\overline{D}$ cross sections are about equal. On the other hand, e^+e^- annihilation data indicates that $67 \pm 10\%$ of the charmed quarks fragment into D mesons [9]. Accounting for D_s states leaves little room for charmed baryon production in e^+e^- annihilation. The measured $e^+e^- \to \Lambda_c X$ cross section [10] also suggests, within rather large uncertainties, that charmed baryons are produced less frequently than charmed mesons in e^+e^- annihilation. Thus the comparison of the e^+e^- data with the ACCMOR results again implies a breakdown of QCD factorization.

The coalescence of light and charmed quarks results in large factorization–breaking enhancements of $\Lambda_c(cud)$ production in pp collisions at large x_f since the charmed baryon can carry two of the projectile valence quarks. The ISR charmed baryon production data indicates Λ_c production at large x_f [11]. In the most recent analysis [12], $dN(pp \to \Lambda_c X)/dx_f \propto (1-x_f)^n$ with $n \sim 2.1$. This broad distribution suggests that the charmed baryon receives part of its momentum from the coalescence of the charmed quark with valence partons. In the hyperon beam experiment, $\Sigma^-(dds)\mathrm{Be} \to \Xi_c^+(csu)X$, Biagi *et al.* [13] have reported broad production cross sections at large x_f, $n = 1.7 \pm 0.7$ for Ξ_c^+ production with $x_f > 0.6$. This suggests that the momentum of the incident strange quark contributes to the momentum of the final–state charmed–strange baryon.

Nuclear targets provide a particularly sensitive test of QCD factorization. The nuclear dependence of heavy quark production is usually parameterized as

$$\sigma_{hA \to Q\overline{Q}} = \sigma_{hN \to Q\overline{Q}} A^{\alpha} \ . \tag{2}$$

Leading–twist QCD factorization applied to hA reactions predicts that any variation from a linear dependence on A arises solely from the nonadditivity of the nuclear structure function, $G_{a/A}(x,Q^2) \sim A^{\alpha(x)} G_{a/N}(x,Q^2)$. The A dependence of J/ψ production shows a decrease in α with the J/ψ momentum fraction x_f. The data [14,15,16] at different energies show that $\alpha = \alpha(x_f)$ rather than $\alpha = \alpha(x_b)$, as predicted by Eq. (1), thus violating QCD factorization [17].

This anomalous nuclear dependence of J/ψ production cannot be explained as the effect of final–state absorption of the charmonium state for several reasons. First, for-

mation time and color transparency arguments show that the $c\bar{c}$ system hadronizes at a distance proportional to its laboratory energy [18]; thus less attenuation is predicted as x_f increases, directly opposite to observation [19]. In addition, the measured attenuation of the J/ψ and ψ' observed by E772 are nearly identical [16] despite their different transverse sizes. It is also difficult to explain the nuclear attenuation at large x_f as solely the effect of energy loss by the initial or final state quarks or gluons [20], compatible with the remarkably low nuclear degradation of the final state jet seen in leptoproduction [21]. In Ref. [22] a quantum mechanical bound for the energy loss $dE/dz \sim 0.6$ GeV/fm is given, too low to explain the nuclear effect seen in J/ψ production. Furthermore, one can show on general grounds that the laboratory energy loss of the incident parton should be the same in both Υ and J/ψ production, in contradiction to the much smaller nuclear effect for $b\bar{b}$ systems seen by E772 [16].

The A dependence of open charm production is less well determined, but the available data suggest a nuclear suppression increasing with x_f. Beam dump experiments that measure charm production through prompt muon and neutrino detection find $\alpha \sim 0.75 - 0.85$ at relatively large charm x_f [23,24]. On the other hand, A–dependence measurements at CERN which emphasize charm production at lower x_f find $\alpha = 0.89 \pm 0.05 \pm 0.05$ at 340 and 370 GeV with π^- and p beams on Si and W targets [25]. The recent Fermilab experiment E769 [3] also finds a nearly linear A dependence for $\pi^- A$ interactions at low x_f. It should be noted that aside from small corrections due to shadowing of the nuclear structure functions, PQCD predicts $\alpha \cong 1$ at all x_f to leading twist. The evidence that $\alpha(x_f)$ decreases with x_f again suggests the presence of competing higher–twist mechanisms which dominate charm production at large x_f.

The charmonium hadroproduction data have a number of other unexpected features. The cross section measured by NA3 [14] for J/ψ production at large x_f and low p_T appears to have a 'diffractive' contribution in excess of the conventional $gg \to c\bar{c}$ and $q\bar{q} \to c\bar{c}$ fusion prediction. Since the J/ψ does not contain any projectile valence quarks, this excess production at large x_f cannot be explained by a coalescence effect. Measurements also show that the transverse momentum distribution of the J/ψ produced in $\pi^- A$ collisions significantly narrows at high x_f [14,26]. Although the J/ψ is produced with no net polarization at moderate x_f, the J/ψ's produced in π^-W collisions at $x_f > 0.9$ are almost completely longitudinally polarized [26]. These anomalies again suggest that an additional mechanism, not included in leading–twist QCD, contributes to charm production at large momentum fractions.

There is, in fact, an additional mechanism for the production of heavy–quark systems predicted by QCD. Scattering of the projectile in the target can liberate intrinsic $c\bar{c}$ fluctuations, existing over a time $\Delta t = 2P_{lab}/M^2_{Q\bar{Q}}$, from the projectile wavefunction. Materialization of these states leads naturally to Feynman scaling distributions. An intrinsic $|uudc\bar{c}\rangle$ Fock component in the projectile wavefunction can be generated by virtual interactions such as $gg \to c\bar{c}$ where the gluons couple to two or more of the projectile valence quarks. The probability for finding a heavy–quark pair of mass $M_{Q\bar{Q}}$ or greater in the hadron wavefunction generated by this mechanism is of order $\alpha_s^2(M^2_{Q\bar{Q}})/M^2_{Q\bar{Q}}$, with the overall coefficient set by the parton–parton correlation length. Intrinsic charm is thus a higher–twist phenomenon. Viewed semiclassically, the intrinsic

charm Fock components are associated with configurations of the wavefunction having equal velocity constituents. Thus, unlike normal sea quarks generated by evolution from a single parton, the intrinsic charm quarks carry a large fraction of the parent hadron's momentum [27]. Since the quarks in the intrinsic Fock state have similar velocities, coalescence of the charmed quark with projectile fragments will produce leading charmed hadrons. Alternatively, the intrinsic c and $\bar{c}$ can coalesce to produce a charmonium state with the majority of the projectile momentum. Direct measurements of the charm contribution to the structure function $F_2(x)$ by the European Muon Collaboration [28,29] at $Q^2 \leq 75$ GeV^2 and $x_{Bj} \leq 0.42$ suggest that the momentum distribution of charmed quarks in the nucleon is harder than expected from photon–gluon subprocesses or conventional QCD evolution at large x_{Bj}. The analysis of Hoffman and Moore [29] indicates that the probability of finding intrinsic charm Fock states in the proton wavefunction is approximately 0.3%. This is consistent with the upper bound of 0.6% given by the EMC group [28].

If the projectile wavefunction has an intrinsic charm component [27], the x_f dependence of the effective power α in heavy–quark hadroproduction can readily be accounted for. A phenomenological interpretation of the J/ψ A dependence based on the intrinsic charm ansatz was given in Ref. [30]. It was suggested that at large x_f $c\bar{c}$ production is dominated by the intrinsic component [27,31] liberated from its virtual state by interactions of the light spectator quarks in the projectile with the target nucleus. The $c\bar{c}$ cluster, which carries a high momentum fraction and has a small transverse size, passes through the nucleus undeflected, evolving into charmonium states after transiting the nucleus. As we discuss below, the remaining cluster of light quarks in the Fock state carries a low momentum fraction, interacts strongly, and thus tends to be absorbed on the front surface of the nucleus. The nuclear cross sections will thus be surface dominated, *i.e.* $\alpha(x_f) \to 2/3$ at large x_f, as seen in the data [14,15,16,32]. We emphasize that this nuclear dependence is unrelated to the shadowing of parton distributions.

The role of the various leading– and higher–twist contributions to heavy quarkonium production was systematically analyzed in a specific gauge theory model in Ref. [1]. It was shown that virtual $c\bar{c}$ or lepton pairs can be liberated at large x_f by a relatively soft interaction with a light quark component of the projectile. The hardness of the interaction scales as $M^2_{Q\bar{Q}}(1-x_f)$, where $M_{Q\bar{Q}}$ is the pair mass and the liberation probability is proportional to $1/[M^2_{Q\bar{Q}}(1-x_f)]$. The coherence of the intrinsic Fock state is easily broken by soft interactions with small transverse momentum since the transverse velocity given to the spectators, $v_\perp = p_\perp/p(1-x)$, is large. Because of the rapid transverse expansion of the spectators, production cross sections in nuclear targets become surface dominated at large x_f.

The change in physics from volume dominated leading–twist fusion subprocesses to surface dominated higher–twist intrinsic charm contributions thus occurs as x_f increases. The leading contributions to the production cross section at large x_f actually come from spectator interactions rather than direct interactions with the pair itself, and at sufficiently large x_f, the cross section for freeing the pair becomes large enough so that an x_f–dependent departure from A^1 behavior can be expected. We emphasize that the predicted A dependence of the production cross section in the fixed $(1-x_f)M^2_{Q\bar{Q}}$ limit

is a function of x_f rather than a function of the target momentum fraction x_b. Clearly leading–twist perturbative QCD factorization is invalid in this limit since there is no relative suppression of interactions involving several constituents of the same hadron.

The intrinsic charm model, backed up by perturbation theory [1] in the fixed $(1 - x_f)M^2_{Q\overline{Q}}$ limit, thus justifies the analysis of Badier *et al.* [14] in which 'hard' and 'diffractive' contributions to charmonium production in πA and pA collisions were separated on the basis of their dependence on the nucleon number of the target:

$$\frac{d\sigma(hA)}{dx_f} = A^{\alpha'}\frac{d\sigma_{\rm pf}}{dx_f} + A^{\beta}\frac{d\sigma_{\rm ic}}{dx_f} \simeq A^{\alpha(x_f)}\frac{d\sigma(hN)}{dx_f} \ . \tag{3}$$

The first component $\sigma_{\rm pf}$, dominant at moderate values of x_f, is the perturbative QCD model of parton fusion. This component has an almost linear A dependence, modulo small nuclear shadowing corrections. Because of QCD factorization, any final state absorption effect should be a higher–twist contribution. The second component $\sigma_{\rm ic}$, which dominates at high x_f, is assumed to arise from an intrinsic heavy quark component of the projectile freed by the interactions of the spectator partons at the nuclear surface. This gives rise to a near $A^{2/3}$ dependence ($\beta = 0.77$ for pion and $\beta = 0.71$ for proton beams). The effective x_f dependent power $\alpha(x_f)$ seen in charmonium production is thus explained by the different characteristics of the two production mechanisms. Hard gluon fusion production dominates at small x_f due to the steeply falling gluon structure function. The contribution from intrinsic charm Fock states peaks at higher x_f due to the large momentum carried by the charmed quarks. This two component model also explains why the nuclear dependence of J/ψ production depends on x_f rather than on x_b as predicted by leading–twist factorization [17]. Another important consequence of this picture is that all final states produced by a penetrating intrinsic $c\bar{c}$ component will have the same A dependence. In particular, the ψ' will exhibit the same behavior as the J/ψ in spite of its larger size. This is confirmed by the recent E772 data [16]. The nucleus cannot influence the quark hadronization taking place outside the nuclear environment at high energies.

In our previous paper [33], we presented an analysis of the existing data for hidden charm production based on the two component model summarized in Eq. (3). Using plausible parameters, we were able to account for both the x_f and A dependence of J/ψ production. In our analysis it was essential to take into account the effect of the interaction of the produced c or $\bar{c}$ with comoving spectators, especially in nuclei[18,33,34]. In particular, the production of a $c\bar{c}$ bound state at low x_f will be attenuated due to coalescence of the produced c or $\bar{c}$ with these spectators, producing charmed hadrons at the expense of charmonium survival. Because the J/ψ cross section is smaller than the open charm production cross section, this conversion of hidden to open charm only affects the open charm production probability at the 2% level. In the present work we shall discuss another effect of comover interactions. In e^+e^- annihilation the charmed quark is decelerated due to light quark pair production. However, the availability of comoving light quarks in hadronic reactions allows the charmed quark to maintain its velocity as it coalesces to form a charmed hadron.

It should be emphasized that in leading–twist QCD the universality of the fragmen-

tation function $D_{H/q}(z,Q^2)$, *i.e.* its independence of the target and projectile identity, occurs because the parton is produced at large transverse momentum in a kinematic region clear of the spectator partons or hadrons created from beam and target fragmentation. One expects marked changes in the physics when these kinematic conditions are not fulfilled. For example, in QED, Bethe–Heitler pair production in a nuclear collision is strongly modified by the attractive forces between the produced electron and the highly charged nucleus. The Coulomb forces are particularly strong when the charges have similar velocities, leading to the electron binding with the comoving nucleus [35]. Similarly in QCD, a quark can hadronize by coalescing with a comoving spectator parton [36]. The effect is clearly enhanced in nucleus–nucleus collisions, especially in events with large global transverse energy, E_T. As discussed in Refs. [33,34], comover interactions can account for the observed decrease [37] of the J/ψ to continuum $(\mu^+\mu^-)$ ratio with E_T seen in nucleus–nucleus collisions as well as the suppression of J/ψ and Υ production seen at negative x_f in pW collisions [38]. Just as in photon–induced capture reactions [39] the effect could be nonlinear in the number of comoving spectators. A comprehensive discussion of the systematics of charmonium production based on fusion processes, intrinsic charm, and comover interactions, including detailed predictions for heavy–quarkonium suppression by comover interactions in relativistic heavy–ion collisions, is given in Ref. [33].

In this paper we shall study the consequences of these same physical effects on the production of open charm. In particular, we investigate the effects of comover coalescence on the momentum distribution of the charmed hadrons. According to the QCD factorization theorem, the charmed quark fragmentation function, $D_{H/c}(z,Q^2)$ can be taken directly from e^+e^- data. This prediction severely underestimates the observed production of charmed hadrons at moderate to large x_f. As discussed above, the physical origin of this effect could be comover interactions since the coalescence of the charmed quark with a comoving spectator of low relative velocity can add to the net momentum of the charmed hadron. This factorization–breaking effect should be most important for charmed hadrons produced at low transverse momentum relative to the beam direction.

At the largest values of x_f, one must understand the mechanisms for the transfer of momentum from energetic valence quarks to the charmed quarks. This process is in principle calculable from perturbative QCD using the methods of Ref. [1]. Such a calculation has, however, not yet been attempted. Thus we use the original, semiclassical intrinsic charm distributions [27] based on the energy denominators that emphasize quark configurations in which the constituents have equal velocities. The normalization of the intrinsic charm component is the same as in our previous study [33] of quarkonium production.

The plan of this paper is as follows: First we describe the calculation of the charm production cross section in the fusion model. We then determine the distribution of charmed hadrons created from the liberation of intrinsic heavy quark states. We have explored several ways to incorporate intrinsic charm into the model, but in each case we assume that the percentage of the open charm production cross section due to intrinsic charm is identical to that describing the relative contribution to J/ψ production. Our

calculations are then compared to the x_f and A dependence of the hadroproduction data. We also compute in some detail the single lepton yield resulting from semi-leptonic decays of open charm. These leptons are important as a background to signals of quark–gluon plasma formation in nucleus–nucleus collisions. A substantial part of the dilepton continuum below the J/ψ mass is due to $D\overline{D}$ decays. Unless the detailed characteristics of open charm production in a nuclear environment are known, it will be difficult to separate the physics of semileptonic D decays from the Drell–Yan lepton pair formation or from a more exotic signal resulting from quark–gluon plasma creation. Charm production will thus play a crucial role in deciphering RHIC physics.

Charmed Hadrons from Parton Fusion

We begin by calculating the doubly inclusive cross section for charmed hadron production in hadron–hadron collisions. The charmed quarks are produced via the subprocess $a + b \rightarrow 1 + 2$ where 1 and 2 are the produced charmed quarks and a and b are the colliding partons, either quarks or gluons, from incident hadrons A and B. The charmed quarks subsequently fragment into charmed hadrons, *i.e.* $1 \rightarrow 3$ and $2 \rightarrow 4$. The doubly inclusive cross section for charmed hadron production is given by

$$E_3E_4\frac{d\sigma_{\rm pf}}{d^3p_3d^3p_4} = \int \frac{\hat{s}}{2\pi}\frac{dx_a}{x_a}\frac{dx_b}{x_b}dz_3dz_4H_{ab}(x_a,x_b)\frac{E_3E_4}{E_1E_2} \frac{D_{H/c}(z_3)}{z_3^3}\frac{D_{\overline{H}/\bar{c}}(z_4)}{z_4^3}\delta^4(p_a+p_b-p_1-p_2)\ , \tag{4}$$

with

$$H_{ab}(x_a,x_b) = \sum_{a,b}(q_a(x_a)\bar{q}_b(x_b) + \bar{q}_a(x_a)q_b(x_b))\frac{d\hat{\sigma}}{d\hat{t}}|_{q\bar{q}} + g_a(x_a)g_b(x_b)\frac{d\hat{\sigma}}{d\hat{t}}|_{gg}\ , \tag{5}$$

where x_a and x_b are the parton momentum fractions and $q(x)$ and $g(x)$ are the quark and gluon structure functions of the incident hadrons. The derivation is given in Appendix A. For the nucleon, we use set B of the recent determination of the structure functions by Harriman *et al.* with $\Lambda_{\rm QCD} = 0.19$ GeV and $xg_p(x) \propto (1-x)^5$ [40]. For the pion, we use a set determined by Badier *et al.* with $xg_\pi(x) \propto (1-x)^{2.4}$ fit from hard perturbative J/ψ production data [14]. The hadronic center–of–mass energy squared, $s = (p_A + p_B)^2$, and that of the colliding partons, $\hat{s}$, are related by $\hat{s} = x_ax_bs$ with $\hat{s} > 4m_c^2$ where $m_c = 1.5$ GeV is the charmed quark mass. The subprocess cross sections $d\hat{\sigma}/d\hat{t}$ have been calculated to next–to–leading order in α_s [41,42,43].

In our calculations we have used the lowest order $q\bar{q} \rightarrow c\bar{c}$ and $gg \rightarrow c\bar{c}$ subprocess cross sections with $\alpha_s = 0.27$ and allowed for an overall K factor to obtain the correct normalization of the total cross section. The differential distributions are not significantly changed by the inclusion of higher–order processes [42]. Uncertainties due to the choice of renormalization scale and the value of the heavy quark mass are thus avoided.

In the next–to–leading order heavy–quark calculations, the K factor determined from the ratio of the $\mathcal{O}(\alpha_s^3)$ cross section to that of lowest order was found to be ~ 3, which is the factor needed to account for the normalization of the data [44].

The fragmentation of the charmed quark into a charmed hadron is described by the variable z,

$$z_3 = |\vec{p_3}|/|\vec{p_1}| \ , z_4 = |\vec{p_4}|/|\vec{p_2}| \ . \tag{6}$$

The momentum of the produced hadron is assumed to be collinear with that of the charmed quark. We study the hadronization process using two different functional forms for the fragmentation function $D_{H/c}(z)$. In delta function fragmentation,

$$\delta: \quad D_{H/c}(z) = \delta(1-z) \ , \tag{7}$$

all the heavy quark momentum is transferred to the produced hadron. In Peterson fragmentation [45], we use a form which describes D production data in e^+e^- collisions,

$$\mathrm{P}: \quad D_{H/c}(z) = \frac{N}{z(1-1/z-\epsilon_c/(1-z))^2} \ , \tag{8}$$

where $\epsilon_c = (m_q/m_c)^2 = 0.06$ is fit from e^+e^- data [46] and the normalization N is defined by $\sum_H \int D_{H/c}(z)dz = 1$. The prediction of QCD factorization at leading twist is that the fragmentation function is independent of the production process. Therefore the Peterson function obtained from the e^+e^- data represents the leading–twist PQCD prediction. The delta function case approximates a physical situation where the charmed quark coalesces with a light spectator quark from the projectile so that the charmed quark retains its velocity. This factorization–breaking phenomena is only expected to occur when the charmed hadron is produced at low p_T in the forward direction, *i.e.* when it is aligned with the spectators.

The Peterson fragmentation process decelerates the charmed quark during hadronization, making the x_f dependence more central for charmed hadrons than for the charmed quarks. Fig. 1 shows a typical example of $d\sigma_{\mathrm{pf}}/dx_f$ in 400 GeV pp collisions with Peterson function (solid line) and delta function fragmentation (dashed line). The Peterson function is shown to decrease $\langle x_f \rangle$ by $\sim$ 30% compared to the delta function. Note that the LEBC–EHS data for $pp \to D/\overline{D}\,X$ [47] lies well above the PQCD prediction based on the Peterson function fragmentation. It even lies above the delta function fragmentation model, suggesting that additional mechanisms beyond fusion and coalescence exist.

Parton fusion mechanisms alone also cannot produce the quantum number correlations of leading charm reported in Ref. [4] since lowest–order parton fusion does not favor c over $\bar{c}$ production. In $\pi^- p$ collisions [4], there appears to be a distinction between D's which contain the pion valence quarks (D^-, D^0) and those which do not (D^+, $\overline{D}^0$). Next–to–leading order calculations do predict a small charge asymmetry due to $qg \to Q(\overline{Q})\,X$ and $q\bar{q} \to Q(\overline{Q})\,X$ interference which leads to an enhancement of $\bar{c}$ over c production at large x_f. The size of this predicted enhancement is $\sim$ 10-15% for $x_f > 0.6$ [42,43]. However this charge asymmetry should not be confused with leading charm production which depends on the projectile valence quarks. Coalescence of a charmed quark

produced by the fusion process with a projectile valence quark automatically results in quantum number correlations between the charmed hadron and the projectile. However, the fusion process cannot produce charmed hadrons at very large x_f. Thus the leading charmed particle effect for the largest x_f must arise from some other production mechanism. An intrinsic charm component of the projectile wave function leads to charm production at large x_f. As we shall show, the inclusion of intrinsic heavy quark states can boost the x_f dependence to explain both the shape of the inclusive data as well as producing quantum number correlations of the leading charmed particles.

Charmed Hadrons from Intrinsic Charm

The hadronic wavefunction of the projectile is predicted in perturbative QCD to contain virtual heavy quark pairs with a higher–twist suppression of $\mathcal{O}(1/m_Q^2)$ [1,27]. An example of an intrinsic Fock component arising from multigluon interactions in the proton is shown in Fig. 2. The normalization of the intrinsic components should be computable using effective Lagrangian methods [48]. For each Fock state, momentum conservation implies $\sum_i \vec{k}_{\perp i} = 0$ and $\sum_i x_i = 1$, where $k_{\perp i}$ and x_i are the transverse momentum and fractional (light–cone) longitudinal momentum carried by each constituent of the hadron. The general form of the Fock state wavefunction at fixed light–cone time is

$$\Psi(x_i, \vec{k}_{\perp i}) = \frac{\Gamma(x_i, \vec{k}_{\perp i})}{m_h^2 - \sum_{i=1}^n ((\vec{k}_\perp^2 + m^2)/x)_i} , \tag{9}$$

where Γ is a vertex function computed nonperturbatively, m_h is the hadron mass, and m_i is the mass of each constituent parton. The denominator is minimized when the heaviest constituents carry the greatest fraction of the hadron's longitudinal momentum, equivalent to all constituents of a moving bound state having the same rapidity. Since the constituents tend to have the same velocity in the bound state, the heavy quarks carry the largest fraction of the projectile momentum, $\langle x_Q \rangle > \langle x_q \rangle$, implying an important contribution to charm production at large x_f. For simplicity we will take Γ as a constant [27].

The charmed quarks in the intrinsic charm Fock state are freed in a hadronic collision through the soft interactions of the light quarks in the target [1]. The differential cross section corresponding to an n–particle Fock state (integrated over $k_{\perp i}$) then has the form

$$\frac{d\sigma_{\rm ic}}{dx_1 \ldots dx_n} = N_n \frac{\delta(1 - \sum_{i=1}^n x_i)}{(m_h^2 - \sum_{i=1}^n (\widehat{m}_i^2/x_i))^2} , \tag{10}$$

where $\widehat{m}_i = \sqrt{\langle \vec{k}_{\perp i}^2 \rangle + m_i^2}$ is the average transverse mass and N_n is a normalization factor. In this model $\langle k_\perp^2 \rangle$ is proportional to the square of the quark mass. The inverse square power, appropriate for a higher–twist component, includes the $(1/m_Q^2)$ suppression in

the cross section due to the resolution of the intrinsic heavy quarks. We have assumed the effective values $\widehat{m}_q = 0.45$ GeV for the valence quarks and $\widehat{m}_c = 1.8$ GeV for the charm quarks. Then the x distribution of intrinsic c quarks in a proton–induced interaction is

$$\frac{d\sigma_{\rm ic}}{dx_c} = \int dx_1 dx_2 dx_3 dx_{\bar{c}} \frac{d\sigma_{\rm ic}}{dx_1 \ldots dx_c} \ , \tag{11}$$

where x_1, x_2, and x_3 represent the momentum fractions carried by the valence quarks. (The exact form of $d\sigma_{\rm ic}/dx_c$ as well as all x distributions described in this section can be found in Appendix B.)

We explore several ways to apply the intrinsic charm model to the production of charmed hadrons. First, and perhaps most naturally, the intrinsic heavy quarks are assumed to fragment into hadrons in the same way as $c\bar{c}$ states produced by parton fusion. We will thus consider both the Peterson function, Eq. (8), and delta function fragmentation, Eq. (7). We refer to this as intrinsic fragmentation. For example, $D\overline{D}$ states can be formed from intrinsic charm by this mechanism. The contribution to the D meson x_f distribution due to the fragmentation of the c quark into a D meson is given by

$$\frac{d\sigma_{\rm ic}}{dx_D} = \int dx_c dz_3 D_{D/c}(z_3) \frac{d\sigma_{\rm ic}}{dx_c} \delta(x_D - z_3 x_c) \ , \tag{12}$$

where x_c is the fraction of the projectile momentum carried by the c quark and z_3 is the fraction of the heavy quark momentum carried by the produced hadron, *i.e.* $z_3 = x_D/x_c$. This definition of z is identical to the one given in Eq. (6) if, as we shall assume, the charmed hadron is collinear with the c quark. We obtain the intrinsic c–quark distribution in a proton, $d\sigma_{\rm ic}/dx_c$, by integrating the $|uudc\bar{c}\rangle$ Fock state cross section over the x distributions of the light valence quarks and the $\bar{c}$ quark as in Eq. (11). Fig. 3(a) gives the resulting intrinsic charmed hadron distribution in proton interactions. The solid curve shows the result for the Peterson function while the dashed curve gives our result with delta function fragmentation. When the delta function is used, $d\sigma_{\rm ic}/dx_D = d\sigma_{\rm ic}/dx_c$, whereas the average D momentum is reduced by 33% in Peterson fragmentation. Fig. 3(b) gives the corresponding results for intrinsic charm states from π^- interactions. Note that $\langle x_f \rangle$ is $\sim 20\%$ larger for π production than for protons.

The coalescence of one or both of the intrinsic charm quarks with spectator valence quarks of the Fock state leads in a natural way to leading charmed hadrons at large x_f. If both the c and $\bar{c}$ recombine with valence quarks of the proton, one obtains a leading $\Lambda_c \overline{D}$ combination. Thus the intrinsic $c\bar{c}$ state of the proton $|uudc\bar{c}\rangle$ may recombine with the valence quarks to produce charmed hadrons: $|udc\rangle$ $|u\bar{c}\rangle$ and $|uuc\rangle$ $|d\bar{c}\rangle$, resulting in $\Lambda_c^+ \overline{D}^0$, $\Sigma_c^+ \overline{D}^0$, and $\Sigma_c^{++} D^-$ combinations. This type of coalescence or recombination is particularly natural in the intrinsic charm picture since the valence quarks of the Fock state move with the same velocity as the charmed quarks and have small transverse momentum [1]. The x_{Λ_c} distribution of a Λ_c produced by recombination with proton

valence quarks is calculated from

$$\frac{d\sigma_{\rm ic}}{dx_{\Lambda_c}} = \int \prod_{i=1}^{5} dx_i \frac{d\sigma_{\rm ic}}{dx_1 \ldots dx_5} \delta(x_{\Lambda_c} - x_1 - x_2 - x_c) \ , \tag{13}$$

and is shown in Fig. 4(a). In this scenario, the Λ_c is produced with $\langle x_{\Lambda_c} \rangle = 0.58$. The $\overline{D}$ distribution is obtained when $\delta(x_{\overline{D}} - x_3 - x_{\bar{c}})$ is substituted for the Λ_c delta function. The result, shown in Fig. 4(b), with $\langle x_{\overline{D}} \rangle = 0.42$, produces $\overline{D}$'s at larger x_f than those arising from intrinsic fragmentation. Note that if both the c and $\bar{c}$ recombine, $d\sigma_{\rm ic}/dx_{\Lambda_c} = d\sigma_{\rm ic}/dx_{\overline{D}}$ at $x_{\Lambda_c} = 1 - x_{\overline{D}}$.

Similarly, recombination of an intrinsic $c\bar{c}$ state with valence quarks of the pion will result in the production of D and $\overline{D}$ mesons which are not charge conjugates. We take the example of a π^-, often used as a projectile. The $|d\bar{u}c\bar{c}\rangle$ state may coalesce into $|\bar{u}c\rangle$ and $|d\bar{c}\rangle$, D^0 and D^- mesons. In this case, the resulting meson distributions are symmetric around $x_{D^-} = 0.5$, as shown in Fig. 4(c). The recombination mechanism automatically produces a large leading charm effect for D^0 and D^- mesons, but not for the charge conjugates.

The production of correlated $D\overline{D}$ pairs has been measured in the proton–emulsion experiment of Ref. [49]. The $D\overline{D}$ pair distribution $d\sigma_{\rm ic}/dx_{fp}$, where $x_{fp} = x_D + x_{\overline{D}}$, may be calculated from $c\bar{c}$ states created through parton fusion as well as those produced from intrinsic charm states. Correlated $D\overline{D}$ pairs may arise through intrinsic fragmentation of both heavy quarks,

$$\text{IF}: \quad \frac{d\sigma_{\rm ic}}{dx_{fp}} = \int dz_3 dz_4 D_{H/c}(z_3) D_{\overline{H}/\bar{c}}(z_4) dx_1 \ldots dx_{\bar{c}} \frac{d\sigma_{\rm ic}}{dx_1 \ldots dx_{\bar{c}}} \times \delta(x_{fp} - z_3 x_c - z_4 x_{\bar{c}}) \ , \tag{14}$$

where $x_D = z_3 x_c$ and $x_{\overline{D}} = z_4 x_{\bar{c}}$, as well as from fragmentation of the c quark into a D meson and recombination of the $\bar{c}$ with a valence quark,

$$\text{IF} + \text{R}: \quad \frac{d\sigma_{\rm ic}}{dx_{fp}} = \int dz_3 dx_{\overline{D}} D_{H/c}(z_3) dx_1 \ldots dx_{\bar{c}} \frac{d\sigma_{\rm ic}}{dx_1 \ldots dx_{\bar{c}}} \times \delta(x_{\overline{D}} - x_2 - x_{\bar{c}}) \delta(x_{fp} - z_3 x_c - x_{\overline{D}}) \ . \tag{15}$$

Results for the production of a $D\overline{D}$ pair from intrinsic fragmentation according to Eq. (14) in proton–induced interactions are shown in Fig. 5(a). The result for the delta function form of $D_{H/c}(z)$ is given by the dashed line while Peterson fragmentation is represented by the solid line. The distributions resulting from intrinsic fragmentation and recombination, Eq. (15), is given in Fig. 5(b) for proton interactions. Delta function fragmentation of the c quark is shown by the dashed line and Peterson fragmentation by the solid curve. The combination of intrinsic fragmentation with recombination usually produces hadron pairs at larger x_f than intrinsic fragmentation.

Hadroproduction Results

The total x_f distribution of charmed hadrons produced in hadronic collisions in our model is given by the sum of contributions from parton fusion and intrinsic charm, see Eqs. (4) and (10):

$$\frac{d\sigma_{hN\to c\bar{c}}}{dx_f} = \frac{d\sigma_{\rm pf}}{dx_f} + \frac{d\sigma_{\rm ic}}{dx_f} \ . \tag{16}$$

The cross sections calculated from the fusion processes include a normalization factor $K \sim 2-3$, depending on the center–of–mass energy and projectile hadron [44], since we have only included lowest–order processes. As a first estimate of the normalization of the intrinsic charm component, we assume that the ratio of intrinsic charm to the total open charm cross section is identical to the rate of 'diffractive' to total cross section measured by NA3 for J/ψ production. This gives $\sigma_{\rm ic}/\sigma_{c\bar{c}}^{\rm total} = 0.18$ for pion–nucleon collisions at $p_{\rm lab} = 150 - 280$ GeV/c [14] and $\sigma_{\rm ic}/\sigma_{c\bar{c}}^{\rm total} = 0.11$ for proton–induced reactions at $p_{\rm lab} = 200$ GeV/c [33]. As the energy increases we shall assume that the intrinsic charm cross section scales proportionally to the total inelastic cross section evaluated at $\hat{s} = (1 - x_f)s$. This is suggested by the mechanism to free intrinsic charm discussed in Ref. [1] where the interaction in the target is soft.

For π^-–induced charm production, we shall focus on $D\overline{D}$ production. In addition to the fusion process, the D^+ and $\overline{D}^0$ may be produced from intrinsic fragmentation, while D^0 and D^- states arise from both intrinsic fragmentation and valence quark recombination. The D^0 and D^- mesons are thus referred to as 'leading' D's while the D^+ and $\overline{D}^0$ are 'nonleading'. As a working assumption we set the mixture of leading D's produced by intrinsic fragmentation and recombination at 50% for each. Recent results from the ACCMOR collaboration [8] have shown that $\sigma(\Lambda_c)/\sigma(\bar{\Lambda}_c) \sim 1$, as expected from this model, since the Λ_c and $\overline{\Lambda}_c$ can each carry one π^- valence quark and the fragmentation process gives identical Λ_c and $\overline{\Lambda}_c$ distributions. A comparison of the total pion–induced charm production cross section with the theoretical normalization has to include $D\overline{D}$, $\Lambda_c\overline{\Lambda}_c$, and other associated charm pair states. Thus evaluations of the K factor for fusion processes based on $D/\overline{D}$ data alone may underestimate its size.

A leading charm effect is predicted by the model and can be compared to the 360 GeV $\pi^- p$ bubble chamber data of LEBC–EHS [4]. Calculations of the single particle $D/\overline{D}$ distribution are shown in Fig. 6. The solid curve in Fig. 6(a) is the prediction of PQCD using the standard Peterson fragmentation model. It tends to fall below the data for $x_f > 0.5$. Although the description of the shape is unsatisfactory, the normalization of the fusion prediction is accurate for the total cross section if $K = 3$. A similar problem is seen in Fig. 1 for pp collisions. We will also show in the next sections that the fusion prediction falls too rapidly with x_f compared to the E769 $\pi^- A \to D/\overline{D}\,X$ data [3,50]. The dashed curve shows the effect of including intrinsic charm fragmentation, using the Peterson fragmentation function. The dot–dashed curve includes the full effect of intrinsic charm, allowing for recombination of the valence quarks with the c or $\bar{c}$ to produce leading D's. In Fig. 6(b) delta function fragmentation is assumed for both fusion and intrinsic charm fragmentation. This allows for the coalescence of the heavy quarks with spectators produced in the collision. Clearly some combination of coalescence and intrinsic charm contributions are needed to describe the data. The data

has also been separated into leading and nonleading components. We have compared our calculation including intrinsic charm fragmentation and recombination with the data for leading D production in Fig. 6(c). The solid curve shows Peterson function fragmentation and the dashed curve delta function fragmentation, under the assumption that $\sigma(D^0/D^-) = \sigma(D/\overline{D})/2$. The recombination of intrinsic charm with the valence quarks allows the model to be compatible with the data for $x_f > 0.5$. The nonleading D^+, $\overline{D}^0$ data is compared to our calculation with fusion plus intrinsic fragmentation using delta function (dashed curve) and Peterson fragmentation (solid curve) in Fig. 6(d).

In proton–induced charm production, the dominant channels are expected to be $D\overline{D}$ and $\Lambda_c\overline{D}$. Studies of Λ_c production in pp interactions by LEBC–EHS [51] suggest that $\sigma(\Lambda_c\overline{D}) \leq \sigma(D\overline{D})/2$ at 400 GeV. Thus we estimate $\sigma(\Lambda_c) = \sigma_{\rm tot}/3$, $\sigma(D) = 2\sigma_{\rm tot}/3$, and $\sigma(\overline{D}) = \sigma_{\rm tot}$ where $\sigma_{\rm tot}$ is the total $c\bar{c}$ production cross section. We expect Λ_c's and $\overline{D}$'s from intrinsic charm states to be produced by both intrinsic charm fragmentation and recombination while intrinsically–produced D mesons arise from intrinsic fragmentation. In Fig. 7(a) we show the full $D/\overline{D}$ distribution [47] compared to calculations using Peterson function fragmentation. The solid line is the result with parton fusion alone. The dashed curve includes intrinsic fragmentation while the dot–dashed result follows from the addition of $\overline{D}$ production by intrinsic fragmentation equally mixed with recombination. Again the prediction of PQCD with the standard charm quark fragmentation function measured in e^+e^- annihilation fails to account for the proton–induced charm data for $x_f > 0.4$. Even including an intrinsic charm contribution does not seem to be sufficient to account for the trend of the large x_f data. Fig. 7(b) shows the same results calculated with the delta function. We find that $\langle x_{D/\overline{D}} \rangle$ increases by 7% with the inclusion of intrinsic fragmentation and by 10% with $\overline{D}$ formation from recombination of the intrinsic charmed quark with a valence quark. Thus, as in the case of the pion–induced data, some combination of coalescence and intrinsic charm production is needed to account for the large x_f data.

Inclusive single charmed hadron distributions have also been measured for each D state individually in pp collisions at 400 GeV [52]. Unfortunately the data sample is not very large and the results are inconclusive due to ambiguous events. The data suggests that the D^+ exhibits the strongest forward production, opposite to what we expect for leading charm; however allowing for ambiguous particle assignments the data show little difference between D and $\overline{D}$ production [52]. The D^- and $\overline{D}^0$ distributions, leading charm states in pp collisions according to our model, are shown in Fig. 7(c). The solid curve shows the results for Peterson fragmentation while the dashed curve uses delta function fragmentation. Recombination increases $\langle x_{\overline{D}} \rangle$ by nearly 15% calculated with Peterson fragmentation. The D^+ and D^0 distributions are compared with our calculations in Fig. 7(d). The calculated distributions are more central than the $\overline{D}$ results since D mesons cannot be produced by valence quark recombination. Again, the solid curve shows Peterson function fragmentation and the dashed delta fragmentation. Clearly more data is needed to see if a leading charm effect emerges in $pp \to D/\overline{D}\,X$.

In Fig. 8, we compare our calculations with pp inclusive single $D/\overline{D}$ production data at 800 GeV [53]. Results with Peterson fragmentation are given in Fig. 8(a). The solid

line illustrates the parton fusion contribution alone, the dashed curve includes intrinsic fragmentation, and the dot–dashed curve includes $\overline{D}$ production by intrinsic fragmentation and recombination. The same calculations for delta function fragmentation are given in Fig. 8(b).

Studies of Λ_c production for $x_{\Lambda_c} > 0.5$ have been carried out at the CERN ISR [12]. We have calculated Λ_c production in pp collisions at $\sqrt{s} = 62$ GeV in the context of our model. The dashed curve in Fig. 9(a) shows the result from parton fusion with Peterson fragmentation. Obviously parton fusion alone is inadequate to explain this data. The result for forward Λ_c production including intrinsic charm fragmentation and recombination of the charmed quark with the valence u and d quarks is given by the solid curve. At such large values of x_{Λ_c}, the fragmentation function chosen plays a small role since the distribution is dominated by valence quark recombination. (For either fragmentation function $\langle x_{\Lambda_c} \rangle \sim 0.65$ when $x_{\Lambda_c} > 0.5$.)

In Fig. 9(a), we have normalized both the data and the calculations to the total cross section for $x_{\Lambda_c} > 0.5$. Our intrinsic charm plus fusion model predicts $\sigma_{pp\to\Lambda_c X}(x_f > 0.5) = 0.2\ \mu$b. This is compatible with an extrapolation of the LEBC–EHS data [4]. However, the experimental Λ_c cross section reported by Chauvat *et al.* is $B\sigma_{pp\to\Lambda_c X} = 2.84 \pm 0.5\,\mu$b [12]. Since $B(\Lambda_c^+ \to \Lambda_s\pi^+\pi^+\pi^-) \sim 1.7\%$, their result is a factor of 675 above our prediction[1]. Although we are not able to account for the normalization of the ISR $pp \to \Lambda_c X$ data, its x_f dependence agrees with our model. The shape of the ISR cross section is also compatible with the Biagi *et al.* result for $\Sigma^- N \to \Xi_c X$ which gives the distribution $(1 - x_f)^{1.7\pm0.2}$ [13].

The cross sections for charmed meson production $pp \to D^+X$ and $pp \to D^0X$ were also measured at the ISR [54]. The most reasonable estimates of the $D\overline{D}$ cross section were obtained assuming that both D's were produced 'centrally' with a $(1-x_f)^n$ distribution with $n = 3$. The D distributions along with our results are given in Fig. 9(b). Results for D production with intrinsic fragmentation included are shown for Peterson function fragmentation (solid curve) and delta fragmentation (dashed curve). Both curves are compatible with the data.

In summary, the existing data for open charm production, although still limited, does not appear compatible with the shapes of the x_f distributions predicted by leading–twist PQCD. The data for $x_f > 0.5$ and the evidence for leading charm quantum number correlations requires other contributions. Our model, which includes delta function fragmentation from coalescence and intrinsic charm, appears to account for the main features of the data (expect for the normalization of the ISR data). We now apply the model to hadron–nucleus interactions.

Nuclear–Dependent Effects

The nuclear dependence of charm production provides a stringent test of the pro-

[1]Note that there is a factor of 50000 difference between the experimental result and that of the parton fusion model with Peterson fragmentation.

duction mechanism. The fusion model is essentially additive in its nuclear dependence,

$$\frac{d\sigma_{\rm pf}(A)}{dx_f} = A^{\alpha'}\frac{d\sigma_{\rm pf}}{dx_f}\ , \tag{17}$$

with $\alpha' \cong 1$ up to small shadowing and antishadowing corrections (which we include). The intrinsic production of charm, as for the total hadron–nucleus cross section, $hA \to X$, tends to occur on the front surface of the nucleus [1]. Hence

$$\frac{d\sigma_{\rm ic}(A)}{dx_f} = A^{\beta}\frac{d\sigma_{\rm ic}}{dx_f}\ , \tag{18}$$

where $\beta = 0.77$ for pion–induced reactions and $\beta = 0.71$ for proton–induced reactions. The A dependence of charm production from intrinsic $c\bar{c}$ states is close to an $A^{2/3}$ surface effect since the light valence quarks have a large transverse size and interact primarily on the nuclear surface. Soft interactions can bring the $c\bar{c}$ pair on mass shell, either as a charmonium bound state, as in the 'diffractive' component of J/ψ production [14], or as a pair of charmed hadrons formed by intrinsic fragmentation or recombination with the projectile valence quarks. In our earlier work [33], we showed that the A dependence of J/ψ production is accounted for by this basic model. In addition we also considered the A–dependent effects of nuclear absorption and interactions with comovers. The comover effect accounts for the depletion of the J/ψ and Υ production at negative x_f in pA collisions seen by E772 [38] as well as the attenuation of the J/ψ to $\mu^+\mu^-$ ratio at large E_T and low p_T seen by NA38 in nucleus–nucleus collisions [37].

The interaction of the nascent $c\bar{c}$ with target nucleons can break up the state before it can escape the target and form a $c\bar{c}$ bound state. Since $c\bar{c}$ pairs produced at large momentum take longer to form bound states, nuclear absorption becomes less effective under these conditions. The comover interaction, corresponding to the coalescence of the $c\bar{c}$ with projectile fragments, also diminishes the probability of the $c\bar{c}$ pair to evolve into a charmonium state. In the case of open charm production, interactions of the $c\bar{c}$ pair with nucleons and comoving light quarks will affect the fragmentation process but does not reduce the number of charmed hadrons produced, thus resulting in $\alpha' = 1$ at the partonic level. Once the charmed hadrons and comoving light hadrons have been formed, they may still interact outside the nucleus to change the charge or baryon number of the charmed mesons and hadrons through exchange reactions such as $\pi^- D^+ \rightleftharpoons \pi^0 D^0$ and $\pi^- \Lambda_c \to D^0 n$, causing a deviation of α' from unity for individual charmed hadrons in hA and AB collisions [55]. In this work, we have used $\alpha' = 1$ as a first approximation. Further studies of exchange cross sections and reaction rates, outside the scope of this work, are necessary before more quantitative conclusions may be reached.

According to QCD factorization, shadowing at fixed target fraction x_t is indifferent to the flavor content of the produced hadron. We set the size of the sea quark shadowing from an analysis of deep–inelastic scattering [56]. Gluon shadowing was treated as in Ref. [33] for J/ψ production. Shadowing is most important for the A dependence of $\sigma_{\rm pf}$ as $\sqrt{s}$ and x_f increase since $x_t = (-x_f + \sqrt{x_f^2 + 4m_c^2/s})/2 \to 0$ for $x_f \gg 4m_c^2/s$. However, the overall effect of shadowing on the combined x_f dependence is small at

high x_f due to the relatively insignificant fusion cross section compared to the intrinsic charm contribution. In addition, since most of the hadron–nucleus charm production data [23,25,47] is at a low average center of mass energy, $\sqrt{s} \sim 25$ GeV, shadowing alone will not have much effect on the A dependence of $\sigma_{\rm pf}$. Thus, given our choice of α', we expect a nearer–to–linear A dependence of charm production by for parton fusion than that found in J/ψ production studies.

In Fig. 10, we show the predicted nuclear dependence of leading charmed meson production for $\pi^- {\rm W} \to D^- X$ relative to $\pi^- p$ production at 250 GeV predicted by the fusion plus intrinsic charm model with Peterson fragmentation. Fusion alone predicts $A^{\rm eff}/A \cong 1$ for all x_f. The effect of intrinsic charm and recombination occurs dominantly at low p_T where the valence and charm quarks are aligned. In order to illustrate this effect, we use the following parameterization of the p_T dependence,

$$\frac{dN_{\rm pf}}{dp_T^2} \propto \frac{1}{(p_T^2 + m_c^2)^2} , \tag{19}$$

$$\frac{dN_{\rm ic}}{dp_T^2} \propto \frac{1}{(p_T^2 + (m_c/2)^2)^4} . \tag{20}$$

The higher–power falloff in the p_T dependence of intrinsic charm reflects its higher–twist nature. Similarly, a smaller scale like $m_c/2$ is expected because recombination occurs with valence quarks at low p_T. The dashed line in Fig. 10 shows that the nuclear attenuation is strongly diminished at large p_T since the contribution of intrinsic charm is suppressed relative to the fusion contribution. In the case of the J/ψ, one also expects that the intrinsic charm contribution occurs at relatively low mean p_T. In the analysis of Ref. [1], $\langle p_T^2 \rangle_{J/\psi}^{\rm intrinsic} \propto (1 - x_f) m_c^2$ was obtained.

As in the case of leading D production above, we expect that the nuclear target suppression for large x_f J/ψ production should diminish with increasing p_T. Such an effect has in fact been observed by several experiments [14,15,26]. In the next section we discuss the available data for charmed hadron production by nuclei. In our comparison with the data we have assumed that the experiments have uniform acceptance in p_T. It should be emphasized that if an experiment has a bias toward large p_T, the effects of intrinsic charm, coalescence, quantum number correlations, and nuclear attenuation will be reduced.

D Production in Hadron–Nucleus Interactions

Charm production studies in hadron–nucleus interactions are of two basic types. The first involves complete reconstruction of the charmed hadron mass from its decay products, often using a vertex detector. The ability to detect charm produced with $x_f \gtrsim 0.5$ in these experiments is limited by their vertex identification capability which requires that the charmed hadrons decay away from the beam. These low x_f experiments report cross sections which have a close to linear A dependence. The second type of experiment involves detection of prompt leptons and neutrinos from charm decays in a

forward beam dump. These studies cannot give reliable x_f distributions of the charmed particles because the identity and momentum of the decaying charm state cannot be unambiguously reconstructed. The bulk of the beam dump data corresponds to charmed hadron production with $x_f > 0.15 - 0.20$. These experiments tend to report significant nuclear attenuation with $\alpha \sim 0.70 - 0.85$.

The model discussed in this paper predicts that leading charm effects are diminished in nuclear targets because of a relative suppression of the intrinsic charm component. As seen from Eq. (18), the large x_f cross section which contains leading particle effects is suppressed by $A^{\beta-1}$. There have been a number of $\pi^- A$ experiments which have searched for leading charm effects [8,25,50]. The D^0, a leading charm state when directly produced, can also be produced by $D^{+\star}$ and $D^{0\star}$ decays; *e.g.* 50% of nonleading $D^{+\star}$'s decay to D^0. Thus in several experiments, only $D^{\pm}$ mesons are used in the analysis to avoid ambiguities. Since the D mass peak is reconstructed from hadronic decays, the best data is at low to moderate x_f. The statistics becomes rather poor above $x_f > 0.5$. Some of these experiments also measure the A dependence of $D^{\pm}$ production [25,50]. The data is presented as the number of charmed particles per x_f bin rather than as an absolute cross section.

The ACCMOR collaboration studied $D^{\pm}$ production in π^-Cu interactions at 230 GeV [8]. In Fig. 11 we compare our calculations with the data for combined $D/\overline{D}$ production as well as that divided into leading and nonleading D's. Although only one nuclear target has been used, we will compare the π^-Cu predictions with calculated $\pi^- p$ results at the same energy in order to illustrate the A dependence of the distributions. In Fig. 11(a) and 11(b) we show the calculated combined distributions in $\pi^- p$ and π^-Cu interactions respectively. The solid curves show our results using Peterson fragmentation for parton fusion alone while the dashed curves include intrinsic charm with contributions from intrinsic fragmentation and recombination with the π^- valence quarks for leading D production. Delta function fragmentation is illustrated in the dotted and dot–dashed curves with and without intrinsic charm contributions respectively. In $\pi^- p$ interactions, including nonleading D production by intrinsic fragmentation increases $\langle x_f \rangle$ by 15% for either fragmentation mechanism while $\langle x_f \rangle$ increases 20% due to valence quark recombination in leading D production. However, the predicted leading charm behavior is suppressed by $\sim 40\%$ for the Cu target due to the '$A^{2/3}$' dependence of intrinsic charm production. It is thus not surprising that a reduced leading contribution is seen in nuclear studies. In Fig. 11(c) and 11(d) we compare the leading and nonleading D distributions with our calculations. The solid and dashed lines show Peterson fragmentation in π^-Cu and $\pi^- p$ interactions. The leading $\overline{D}$ distribution is more influenced by the A dependence of intrinsic charm than the D distribution. The dot–dashed and dotted lines give the same results using delta function fragmentation. Note that it is difficult to explain the moderate x_f data obtained from the nuclear target using the Peterson function.

The x_f distributions, $dN/dx_f = (1/\sigma) d\sigma/dx_f$, are often parameterized by $(1 - x_f)^n$. For leading D production $n = 3.23 \pm 0.29$ while $n = 4.34 \pm 0.35$ for nonleading D production. A fit to the combined data set gives $n = 3.74 \pm 0.23$. Thus a distinction is seen between leading and nonleading D production in the data. Similar results were

obtained for leading and nonleading D^* production. To facilitate a more direct comparison of our model with the experimental results, we estimate n from the average x_f of our calculated distributions: $n = (1/\langle x_f \rangle) - 2$. As expected, n is considerably larger for the more central Peterson fragmentation function with $n = 5.9$ for all D's compared to $n = 3.5$ for the delta function. Hence this nuclear target data supports our earlier conclusion, based on data from nucleon targets, that the charmed hadron x_f distributions are incompatible with the leading–twist QCD prediction (Peterson fragmentation). In nonleading D production, where intrinsic fragmentation is the only intrinsic charm contribution, $n = 3.62$ for the delta function and $n = 6.3$ for Peterson fragmentation. Conversely, for leading D production, we find $n = 3.37$ and 5.67 for delta and Peterson function fragmentation respectively. Thus we deduce $\Delta n \cong 0.25$ between leading and nonleading behavior for the delta function, less than that suggested by the data. This difference in n cannot be accounted for by parton fusion but arises naturally in our model.

In the CERN experiment WA82, charmed hadron production was measured for 340 GeV π^- beams on a combined Si and W target [25]. We compare our calculations with their $D^\pm$ production data in Fig. 12. The curves show the production of charmed mesons per nucleon averaged over the Si and W targets. In Fig. 12(a) we show the combined $D^\pm$ results compared with our calculations using Peterson function fragmentation (solid line) and the delta function (dashed curve). Figs. 12(b) and (c) compare the model with the data separated into leading and nonleading components. The WA82 data for $\pi^- A \to D^\pm X$ has been fit to $(1 - x_f)^n$ with $n = 3.40 \pm 0.45$. The separated $D^\pm$ data suggests the presence of a leading charm effect (with a 10% probability for its absence). The prediction of our model over the same x range is $n = 3.85$ assuming coalescence (delta function fragmentation) and $n = 6.47$ assuming standard Peterson fragmentation. The leading and nonleading charm exponents, n_{D^+} and n_{D^-}, differ by $\sim 10\%$.

The ratio of the total D production cross sections σ_W/σ_{Si} measured by WA82 gives $\alpha = 0.89 \pm 0.05 \pm 0.05$ using Eq. (2). The prediction of our model is $\alpha = 0.97$. Although our model agrees with the WA82 data using intrinsic charm and delta function fragmentation, the absence of information on the nuclear dependence of the differential cross sections and the relative suppression of intrinsic charm at large A makes it difficult to identify the specific effects of intrinsic charm in this data set. However, the prediction of leading–twist PQCD based on fusion and standard Peterson fragmentation is ruled out.

Experiment E769 has measured $D^\pm$ production at 250 GeV in Be, Al, Cu, and W targets [50]. Our calculations are compared with the overall $D^\pm$ production data in Fig. 13. The figures show the number of charmed particles produced per nucleon summed over the four targets. In Fig. 13(a) we show the $D^\pm$ results compared with our calculations using Peterson function fragmentation (dashed line) and the delta function (dot–dashed curve). The result for parton fusion with Peterson function fragmentation alone is shown in the solid curve. Figs. 13(b) and (c) compare the model with the total leading and nonleading data. The solid curves again illustrate the Peterson function while the dashed curves show delta function fragmentation. The nuclear dependence measured by this experiment for $\pi^- A \to D^0 X$ is shown in Fig. 14 [3]. The predicted α

calculated at a similar energy using delta function and Peterson fragmentation is shown in the dashed and solid lines. The deviation of $\alpha(x_f)$ from unity is due to the intrinsic charm component, assuming full p_T acceptance (see Fig. 10). We emphasize that full acceptance down to low transverse momentum will be necessary to check the nuclear attenuation predicted by the intrinsic charm component at large x_f.

We compare our predictions with the E653 data for pairs of charmed particles produced in 800 GeV proton–emulsion interactions [49] in Fig. 15. The fractional momentum of the pair x_{fp} is the sum of those of the charmed mesons. It will be useful to have data at large x_{fp} in order to compare with the measured J/ψ data from E772 [16] and to test predictions of nuclear attenuation. Delta function fragmentation is shown both without intrinsic charm (dashed curve) and with intrinsic charm as calculated from Eqs. (14) and (15), assuming equal contributions from each (dot–dashed curve). Calculations using the Peterson function without (solid curve) and with an intrinsic charm contribution (dotted curve) are also shown. We have assumed that the distribution is symmetric about $x_{fp} = 0$. Because the distributions are normalized to the total rate, the presence of intrinsic charm at forward x_f reduces the magnitude of the fusion contribution at low x_f. At negative x_f the coalescence model predicts nuclear attenuation of J/ψ production due to the presence of comoving nuclear fragments, as observed by E772 [38]. This effect should be absent for charmed hadron production. The apparent symmetry of the distribution in Fig. 15 is compatible with this prediction.

We now focus on A–dependence studies in 'beam dump' experiments where the decay leptons are detected rather than the charmed hadrons themselves. We will discuss only those experiments in which muons are detected. Variable density targets have been used to extrapolate to infinite target density so that muons from semileptonic charm decays are isolated. (Muons from $\pi^{\pm}$ and $K^{\pm}$ decays are suppressed in dense targets because these light hadrons lose energy through interactions within the target before decaying.) Decays of D and Λ_c hadrons contribute to the μ^+ distribution while $\overline{D}$ decays are the primary source of μ^-'s. ($\overline{\Lambda}_c$'s should make a negligible contribution to the forward distribution.) We assume that the branching ratios of charmed hadron decays to muons are approximately the same as those measured for electrons [57]. Taking into account the relative production probabilities for the various D/D^* states, in pA interactions we estimate an effective branching fraction $B(D/D^* \rightarrow \mu^+ X) \sim 0.12$, and use $B(\Lambda_c \rightarrow \mu^+ X) \sim 0.045$. In $\pi^- A$ interactions, the leading particle effects in our model lead to effective branching fractions of ~ 0.163 for charged (D/D^*)'s and ~ 0.077 for neutral (D/D^*)'s. The differences in the distributions of the individual charmed hadrons will result in different behaviors of $\alpha(x_f)$ for μ^+ and μ^-. Muons from leading Λ_c's are suppressed because of the smaller branching ratio.

We will primarily discuss the WA78 experiment which used π^- beams at 320 GeV and proton beams of 300 GeV on Al, Cu, and W targets [23]. The WA78 experiment measures the number of prompt single muons within the range $20 < p_\mu < 100$ GeV. The experimentalists estimated the range of charm momentum by folding the experimental acceptance with a charmed hadron x_f distribution taken from pp collisions, $(1 - x_f)^5$. This indicates charmed hadrons with $x_f \geq 0.1$ were detectable [23]. In the case of π^- collisions, the harder charmed hadron production distribution implies that

the effective range begins at $x_f = 0.2$. The results from WA78 show an appreciable nuclear attenuation. In the case of pA interactions, the nuclear power dependence is $\alpha(\mu^+) = 0.79 \pm 0.12$ and $\alpha(\mu^-) = 0.76 \pm 0.13$. For pion interactions, $\alpha(\mu^+) = 0.76 \pm 0.08$, $\alpha(\mu^-) = 0.83 \pm 0.06$. The experimental result from $\pi^- A$ interactions, averaged over the muon sign, is compared with our calculated average α (as described below) in Fig. 14. The prompt muon signal corresponds approximately to $x_D > 0.2$ and $\langle x_D \rangle \cong 0.4$. This comparison is consistent with the expectation that charm production becomes attenuated in nuclei at large x_f because of the dominance of the intrinsic charm component. We note again that $\alpha \cong 1$ in the PQCD fusion model.

In order to make a comparison with the nuclear dependence of the beam dump data, we have to associate the muons with their respective charmed hadrons. We will infer the charm momentum fraction assuming $x_{f_D} = \kappa x_{f_\mu}$ where $\kappa = 3$. For proton–induced interactions, we take

$$\frac{d\sigma(\mu^+)}{\kappa dx_{f_\mu}} = B(D/D^\star \to \mu^+ X)\frac{d\sigma(D)}{dx_{f_D}} + B(\Lambda_c \to \mu^+ X)\frac{d\sigma(\Lambda_c)}{dx_{f_{\Lambda_c}}} , \tag{21}$$

$$\frac{d\sigma(\mu^-)}{\kappa dx_{f_\mu}} = B(\overline{D}/\overline{D}^\star \to \mu^- X)\frac{d\sigma(\overline{D})}{dx_{f_{\overline{D}}}} . \tag{22}$$

Similarly, for π^-–induced charm production, we have

$$\frac{d\sigma(\mu^+)}{\kappa dx_{f_\mu}} = B(D^0/D^{0\star} \to \mu^+ X)\frac{d\sigma(D^0)}{dx_{f_{D^0}}} + B(D^+/D^{+\star} \to \mu^+ X)\frac{d\sigma(D^+)}{dx_{f_{D^+}}} , \tag{23}$$

$$\frac{d\sigma(\mu^-)}{\kappa dx_{f_\mu}} = B(\overline{D}^0/\overline{D}^{0\star} \to \mu^- X)\frac{d\sigma(\overline{D}^0)}{dx_{f_{\overline{D}^0}}} + B(D^-/D^{-\star} \to \mu^- X)\frac{d\sigma(D^-)}{dx_{f_{D^-}}} . \tag{24}$$

Note that the intrinsic charm contribution is different for D^0 and D^+ in pion–induced interactions. In Fig. 14 we show the predicted nuclear dependence of $\alpha(x_f)$ for the pion beam computed from

$$\alpha = \log(\sigma_{h\mathrm{W}}/\sigma_{hp})/\log(A_\mathrm{W}) . \tag{25}$$

In order to compare with the beam dump results we integrate over the charmed hadron distributions for $x_f > x^D_{\min}$ as predicted by the model. Assuming $x^D_{\min} > 0.2$ we predict $\alpha(\mu^\pm) \sim 0.90$ for Peterson fragmentation and $\alpha(\mu^\pm) \sim 0.92$ for delta function fragmentation. If there were no intrinsic charm contribution, we would expect only a slight deviation from unity, $\alpha(x_f) \sim 0.98$, due to parton shadowing in the fusion contribution.

The prediction of our model for $\alpha(x_f)$ falls between the results of the beam dump [23,24] and active target experiments [3,25]. The discrepancy between the experiments may be due to their different acceptance biases in p_T^D since, as shown in Fig. 10, the contribution from intrinsic charm is mainly at low p_T. In addition, the actual range of the D meson momentum in the beam dump experiments is somewhat uncertain.

Finally, we turn to predictions for experiments at RHIC. Semileptonic decays of $D/\overline{D}$ pairs will be an important part of the background to the electromagnetic di-lepton continuum at $\sqrt{s} = 200$ GeV per nucleon pair. It will be very difficult to detect single D

production without full reconstruction of the D mass. In a dilepton spectrometer, it might be possible to separate $D\overline{D}$ production from dileptons produced by the Drell–Yan mechanism using μe correlations. In this case, the D momentum will remain unknown. We present muon distributions for pp and pAu collisions at $\sqrt{s} = 200$ GeV per nucleon pair, calculated using Eqs. (21) and (22), in Fig. 16. In Fig. 16(a) and (b) we give the μ^- and μ^+ distributions in pp (dashed curve) and pAu (solid curve) for Peterson function fragmentation. The resulting distributions using the delta function appear in Fig. 16(c) and 16(d). The intrinsic charm contribution is greatly reduced at this energy. However, it is responsible for the slight enhancement of the μ^- distribution over that of the μ^+ most apparent in pp collisions. Shadowing is more important at RHIC energies. The pAu cross section per nucleon is 14% smaller than the pp cross section.

B Production in Hadronic Collisions

Our model may also be used to calculate distributions of B mesons. So far, no data is available on the x_f distribution of these mesons. However E789 expects to reconstruct B decays from their pA data at 800 GeV [58]. Due to the large mass of the B meson, shadowing plays a smaller role in the A dependence of B than in D production. In the Peterson fragmentation function, Eq. (8), we must replace ϵ_c by $\epsilon_b = 0.006$, as fit from B meson production in e^+e^- annihilation. The intrinsic beauty contribution is suppressed by a relative factor $(m_c/m_b)^2$, reflecting its higher–twist nature. In pp collisions, B^+ and B^0 mesons are leading since they arise from recombination with proton valence quarks.

In Fig. 17, we show model predictions for pp production of B mesons in an 800 GeV fixed target experiment. Fig. 17(a) and (b) show the distribution of the number of $B/\overline{B}$ mesons produced per x_f using Peterson and delta function fragmentation, respectively. The solid curves show the parton fusion distribution alone, the dashed curves include intrinsic beauty with contributions from intrinsic fragmentation for $\overline{B}$ production and intrinsic fragmentation plus recombination for B production. In Peterson fragmentation, the $\langle x_f \rangle$ of the B meson is 17% smaller than that of the b quark. This deceleration is about half as big as in the charm case. The intrinsic beauty contribution is suppressed relative to intrinsic charm so that its contribution to the distributions is not apparent until $x_f > 0.6$. In fact, including intrinsic beauty increases $\langle x_f \rangle_\delta$ by only 0.4% for both delta and Peterson function fragmentation. Thus intrinsic beauty will only be observable in the high x_f tail of the distribution, making its presence difficult to detect.

In Figs. 17(c) and (d), we show the distributions for leading and nonleading B mesons. In leading B production, shown in Fig. 17(c), the recombination of $\bar{b}$ quarks with proton valence quarks increases $\langle x_B \rangle$ by 0.5% . Nonleading $\overline{B}$ production from intrinsic fragmentation alone is shown in Fig. 17(d). In this case, intrinsic beauty increases $\langle x_{\overline{B}} \rangle$ by $\sim 0.4\%$ for both fragmentation mechanisms.

Conclusions

Charm hadroproduction is a subject of considerable complexity. Although leading–twist PQCD provides rigorous predictions for the production of heavy quarks at sufficiently large p_T, the theory allows for a rich range of phenomena at low transverse momentum where the hadronization process can be strongly modified by interactions and coalescence with the comoving partons produced in the reaction. In addition, the theory predicts the existence of higher–twist heavy quark Fock components which lead to an entirely different type of hidden and open heavy quark hadroproduction. Since the intrinsic heavy quark and the valence quarks in the projectile tend to have parallel and equal velocities, they can recombine to produce heavy hadrons whose quantum numbers are correlated with those of the projectile. Alternatively, the intrinsic Q and $\overline{Q}$ can bind to each other to produce heavy quarkonium states in the large x_f, low p_T kinematic region.

Is this extra complexity allowed by QCD really necessary to explain the existing charm hadroproduction data? As we have shown in this paper, perturbative QCD at leading twist is unable to account for the shape of the x_f distribution, the observed correlation of the leading charmed hadrons with the beam quantum numbers, and the observed nuclear attenuation of quarkonium and heavy hadron production at large x_f. We emphasize that the success of the fusion model in describing charm production cannot be judged solely by the magnitude of the total cross section. All features of the data have to be described. It should also be noted that the magnitude of the cross section predicted by leading–twist QCD is quite uncertain, particularly for charm production. There are ambiguities in the choice of the heavy–quark mass, the argument of the running coupling constant, the parameterization of the quark and gluon structure functions, and the effect of higher–order perturbative corrections which give a K factor ≥ 3. Nevertheless, the predictions of leading–twist QCD should be valid for heavy–quark hadronization at large p_T where coalescence and intrinsic charm effects can be neglected.

Our detailed study shows that the bulk of the charm production data can be understood in terms of a two–component model, consisting of parton fusion with coalescence and intrinsic charm with valence quark recombination. Much more data will be needed to validate this approach and to pin down the model–dependent parameters. In particular, better measurements of x_f, p_T, and A dependence of the open and hidden charm channels are needed. We emphasize that the novel effects due to coalescence and intrinsic charm contribute only in the low p_T region. Experiments that do not have full acceptance in p_T can thus miss some of the essential physics. In fact, a low p_T trigger is most suitable for an intrinsic charm search.

Although our model is consistent with the x_f and A dependence of charmed baryon production, we are not able to account for the high normalization of some of the data. More data on charmed baryon production over the full forward x_f range is needed to resolve this issue.

Charm production will also play a crucial role in looking for new physics in nucleus–nucleus collisions at RHIC. A substantial part of the dilepton continuum below the J/ψ mass will be due to $D\overline{D}$ decays. Unless the detailed characteristics of open charm production in a nuclear environment are known, it will be difficult to separate the physics

of semileptonic D decays from the Drell–Yan mechanism of lepton pair production or from a more exotic signal resulting from quark–gluon plasma formation.

Acknowledgements. We would like to thank J. Appel, S. Gavin, W. Geist, P. Koch, M. Leitch, P. McGaughey, M. Thoma, and G. Young for useful discussions. R.V. would also like to thank Lawrence Livermore National Laboratory for support at the beginning of this work.

References

[1] S. J. Brodsky, P. Hoyer, A. H. Mueller, W.-K. Tang, Nucl. Phys. **B369** (1992) 519.

[2] J. C. Collins, D. E. Soper and G. Sterman, published in *Perturbative QCD*, edited by A.H. Mueller, World Scientific, (1989); G. Bodwin, Phys. Rev. **D31** (1985) 2616, **D34** (1986E) 3932; J. Qiu and G. Sterman, Nucl. Phys. **B353** (1991) 105, *ibid.*, 137.

[3] J. A. Appel, FERMILAB-Pub-92/49, to appear in Ann. Rev. Nucl. Part. Sci. **42** (1992).

[4] M. Aguilar-Benitez *et al.*, Phys. Lett. **161B** (1985) 400, Z. Phys. **C31** (1986) 491.

[5] S. Barlag *et al.*, Z. Phys. **C49** (1991) 555.

[6] R. C. Hwa, Phys. Rev. **D27** (1983) 653.

[7] S. J. Brodsky and J. F. Gunion, Phys. Rev. **D17** (1978) 848.

[8] S. Barlag *et al.*, Phys. Lett. **247B** (1990) 113.

[9] M. Derrick, *Proceedings of the XXIV International Conference on High Energy Physics*, (R. Kotthaus and J. H. Kühn, Eds., Springer 1989), p. 895.

[10] S.R. Klein *et al.*, Phys. Rev. Lett. **62** (1989) 2444.

[11] S. P. K. Tavernier, Rep. Prog. Phys. **50** (1987) 1439; U. Gasparini, *Proceedings of the XXIV International Conference on High Energy Physics*, (R. Kotthaus and J. H. Kühn, Eds., Springer 1989), p. 971.

[12] P. Chauvat *et al.*, Phys. Lett. **199B** (1987) 304 and references cited therein.

[13] S. F. Biagi *et al.*, Z. Phys. **C28** (1985) 175.

[14] J. Badier *et al.*, Z. Phys. **C20** (1983) 101.

[15] S. Katsanevas *et al.*, Phys. Rev. Lett. **60** (1988) 2121.

[16] D. M. Alde *et al.*, Phys. Rev. Lett. **66** (1991) 133.

[17] P. Hoyer, M. Vänttinen, and U. Sukhatme, Phys. Lett. **246B** (1990) 217.

[18] S. J. Brodsky and A. H. Mueller, Phys. Lett. **206B** (1988) 285.

[19] J. Hüfner and M. Simbel, Phys. Lett. **258B** (1991) 465.

[20] S. Gavin and J. Milana, Phys. Rev. Lett. **68** (1992) 1834.

[21] W. Busza, to be published in the proceedings of Quark Matter '91: The Ninth International Conference on Ultra–Relativistic Nucleus–Nucleus Collisions, Gatlinburg, Tennessee, November 11-15, 1991.

[22] S. J. Brodsky, SLAC-PUB-5711 (1991), to be published in the proceedings of Quark Matter '91: The Ninth International Conference on Ultra–Relativistic Nucleus–Nucleus Collisions, Gatlinburg, Tennessee, November 11-15, 1991. S. J. Brodsky and P. Hoyer, in preparation.

[23] H. Cobbaert *et al.*, Phys. Lett. **206B** (1988) 546. H. Cobbaert *et al.*, Phys. Lett. **191B** (1987) 456.

[24] M. E. Duffy *et al.*, Phys. Rev. Lett. **55** (1985) 1816.

[25] M. I. Adamovich *et al.*, CERN preprint, CERN-EP/89-123.

[26] C. Biino *et al.*, Phys. Rev. Lett. **58** (1987) 2523.

[27] S. J. Brodsky, P. Hoyer, C. Peterson, and N. Sakai, Phys. Lett. **93B** (1980) 451; S. J. Brodsky, C. Peterson, and N. Sakai, Phys. Rev. **D23** (1981) 2745.

[28] J. J. Aubert *et al.*, Nucl. Phys. **B213** (1983) 31. J. J. Aubert *et al.*, Phys. Lett. **110B** (1982) 73.

[29] E. Hoffmann and R. Moore, Z. Phys. **C20** (1983) 71.

[30] S. J. Brodsky and P. Hoyer, Phys. Rev. Lett. **63** (1989) 1566.

[31] G. Bertsch, S. J. Brodsky, A. S. Goldhaber, and J. Gunion, Phys. Rev. Lett. **47** (1981) 297.

[32] Yu. M. Antipov, *et al.*, Phys. Lett. **76B** (1978) 235; M. J. Corden, *et al.*, Phys. Lett. **110B** (1982) 415.

[33] R. Vogt, S. J. Brodsky and P. Hoyer, Nucl. Phys. **B360** (1991) 67.

[34] R. Vogt and S. Gavin, Nucl. Phys. **B345** (1990) 104.

[35] C. Bottcher, to be published in the proceedings of Quark Matter '91: The Ninth International Conference on Ultra–Relativistic Nucleus–Nucleus Collisions, Gatlinburg, Tennessee, November 11-15, 1991.

[36] S. J. Brodsky, J. F. Gunion, and D. E. Soper, Phys. Rev. **D36** (1987) 2710.

[37] C. Baglin *et al.*, Can. J. Phys. **67** (1989) 1222.

[38] M. J. Leitch, to be published in the proceedings of Quark Matter '91: The Ninth International Conference on Ultra–Relativistic Nucleus–Nucleus Collisions, Gatlinburg, Tennessee, November 11-15, 1991.

[39] V. B. Berestetskii, E. M. Lifshitz, and L. P. Pitaevskii, *Quantum Electrodynamics, Volume 4, L. D. Landau and E. M. Lifshitz Course of Theoretical Physics*, 2nd Edition (Pergamon Press, Oxford, 1982).

[40] P. N. Harriman, A. D. Martin, W. J. Stirling, and R. G. Roberts, Phys. Rev. **D42** (1990) 798.

[41] R. K. Ellis, lectures give at the 17th SLAC Summer Institute, July 1989, FERMILAB-CONF-89/168-T.

[42] W. Beenakker *et al.*, Nucl. Phys. **B351** (1991) 507.

[43] P. Nason, S. Dawson, and R. K. Ellis, Nucl. Phys. **B327** (1989) 49.

[44] E. L. Berger, in the proceedings of the Advanced Workshop on QCD Hard Processes, St. Croix, 1988.

[45] C. Peterson, D. Schlatter, I. Schmitt, and P. Zerwas, Phys. Rev. **D27** (1983) 105.

[46] J. Chirn, in proceedings of the 'International Symposium on the Production and Decay of Heavy Flavors', Stanford, CA, E. Bloom and A. Fridman Editors, (1987) 131.

[47] M. Aguilar-Benitez *et al.*, Phys. Lett. **189B** (1987) 476.

[48] M. Luke, A. V. Manohar, and M. J. Savage, University of California, San Diego preprint, UCSD/PTH 92-12, 1992.

[49] A. P. Freyberger, Ph. D. thesis, Carnegie Mellon University, 1990, unpublished. K. Kodama *et al.*, Phys. Lett. **263B** (1991) 579.

[50] Zhongxin Wu, Ph. D. thesis, Yale University, 1991, unpublished.

[51] M. Aguilar-Benitez *et al.*, Phys. Lett. **199B** (1987) 462.

[52] M. Aguilar-Benitez *et al.*, Phys. Lett. **210B** (1988) 176.

[53] R. Ammar *et al.*, Phys. Rev. Lett. **61** (1988) 2185.

[54] M. Basile *et al.*, Lett. Nuovo Cimento **33** (1982) 33.

[55] S. Gavin, private communication.

[56] J. Qiu, Nucl. Phys. **B291** (1987) 746.

[57] J. J. Hernandez *et al.*, (Particle Data Group), Phys. Lett. **239B** (1990) 1.

[58] J. Moss, P. L. McGaughey, private communication.

[59] S. Banerjee and S. N. Ganguli, Phys. Rev. **D33** (1986) 1278.

Appendix A

We give a description of the calculation of the charmed hadron distributions within the framework of the parton fusion model [59]. The invariant cross section of the subprocess $a + b \to 1 + 2$ at center–of–mass energy $\hat{s} = (p_a + p_b)^2$ is written as

$$d\hat{\sigma} = \frac{\hat{s}}{2\pi}\frac{d\hat{\sigma}}{d\hat{t}}\frac{d^3p_1}{E_1}\frac{d^3p_2}{E_2}\delta^4(p_a + p_b - p_1 - p_2) \ , \tag{A-1}$$

where $\hat{s}$ is the center–of–mass energy of the colliding partons, $\hat{\sigma}$ is the subprocess cross section, and $\hat{t}$ is the four–momentum transfer squared between the initial partons and the charmed quarks. Neglecting the intrinsic transverse momenta of the incoming partons, we may define the four–momenta of the initial partons, p_a and p_b, the produced charmed quarks, p_1 and p_2, and the charmed hadrons, p_3 and p_4, as

$$\begin{aligned} p_a &= \frac{\sqrt{s}}{2}(x_a, 0, x_a) \ , \\ p_b &= \frac{\sqrt{s}}{2}(x_b, 0, -x_b) \ , \\ p_i &= (\widehat{m}_i \cosh y_i, p_{T_i}, \widehat{m}_i \sinh y_i) \end{aligned} \tag{A-2}$$

where $i = 1, \ldots, 4$, $\sqrt{s}$ is the center of mass energy of the colliding hadrons, $s = x_a x_b \hat{s}$, x_a and x_b are the momentum fraction of the initial hadrons carried by the colliding partons, assumed to be massless, and $\widehat{m}_i$ is the transverse mass of the heavy quarks and final–state hadrons, *e.g.* $\widehat{m}_1 = \sqrt{m_c^2 + p_{T_1}^2}$, where m_c is the charmed quark mass.

We assume that the fragmentation processes $1 \to 3$ and $2 \to 4$ produce charmed hadrons collinear to the charmed quarks. The fragmentation variables are defined as $z_3 = |\vec{p_3}|/|\vec{p_1}|$ and $z_4 = |\vec{p_4}|/|\vec{p_2}|$ with distributions $D_{H/c}(z_3)$ and $D_{\overline{H}/\bar{c}}(z_4)$ respectively. To obtain the inclusive cross section for the production of 3 and 4, the phase space volumes become $d^3p_1 \to d^3p_3/z_3^3$ and $d^3p_2 \to d^3p_4/z_4^3$. Finally, we convolute the subprocess cross sections with the structure functions of partons a and b in the colliding hadrons A and B to find

$$\begin{aligned} E_3E_4\frac{d\sigma}{d^3p_3d^3p_4} &= \int \frac{\hat{s}}{2\pi}\frac{dx_a}{x_a}\frac{dx_b}{x_b}dz_3dz_4H_{ab}(x_a, x_b)\frac{E_3E_4}{E_1E_2} \\ &\quad \frac{D_{H/c}(z_3)}{z_3^3}\frac{D_{\overline{H}/\bar{c}}(z_4)}{z_4^3}\delta^4(p_a + p_b - p_1 - p_2) \ , \end{aligned} \tag{A-3}$$

where

$$H_{ab}(x_a, x_b) = \sum_{a,b}(q_a(x_a)\bar{q}_b(x_b) + \bar{q}_a(x_a)q_b(x_b))\frac{d\hat{\sigma}}{d\hat{t}}|_{q\bar{q}} + g_a(x_a)g_b(x_b)\frac{d\hat{\sigma}}{d\hat{t}}|_{gg} \ , \tag{A-4}$$

with $q(x)$ and $g(x)$ the structure functions of the partons within the hadrons. Using four–momentum conservation to integrate over x_a and x_b, we find

$$E_3E_4\frac{d\sigma}{d^3p_3d^3p_4} = \int \frac{1}{\pi}H_{ab}(x_a, x_b)\frac{E_3E_4}{E_1E_2}\frac{D_{H/c}(z_3)}{z_3^3}\frac{D_{\overline{H}/\bar{c}}(z_4)}{z_4^3}\delta(\vec{p_{T_1}} + \vec{p_{T_2}})dz_3dz_4 \ . \tag{A-5}$$

Transverse momentum conservation gives $\widehat{m}_1 = \widehat{m}_2 = \widehat{m}_c$ and $\widehat{m}_3 = \widehat{m}_4 = \widehat{m}_D$. Then x_a and x_b are defined as

$$x_a = \frac{\widehat{m}_c}{\sqrt{s}}(\exp(y_1) + \exp(y_2)) \ , \tag{A-6}$$
$$x_b = \frac{\widehat{m}_c}{\sqrt{s}}(\exp(-y_1) + \exp(-y_2)) \ .$$

The subprocess cross sections for $c\bar{c}$ production by $q\bar{q}$ annihilation and gg fusion, expressed as a function of $\widehat{m}_c$, y_1, and y_2 are [41]

$$\frac{d\hat{\sigma}}{d\hat{t}}|_{q\bar{q}} = \frac{\pi\alpha_s^2}{9\widehat{m}_c^4} \frac{\cosh(y_1 - y_2) + m_c^2/\widehat{m}_c^2}{(1 + \cosh(y_1 - y_2))^3} \ , \tag{A-7}$$

$$\frac{d\hat{\sigma}}{d\hat{t}}|_{gg} = \frac{\pi\alpha_s^2}{96\widehat{m}_c^4} \frac{8\cosh(y_1 - y_2) - 1}{(1 + \cosh(y_1 - y_2))^3} \left(\cosh(y_1 - y_2) + \frac{2m_c^2}{\widehat{m}_c^2} - \frac{2m_c^4}{\widehat{m}_c^4}\right) \ . \tag{A-8}$$

We have studied the x_f distributions of both single inclusive charm and $D\overline{D}$ pair production. These differential cross sections are give here for completeness. The inclusive x_f distribution ($x_f = 2m_T \sinh y/\sqrt{s}$) of a single charmed hadron ($1 \to 3$) is written as

$$\frac{d\sigma}{dx_f} = \frac{\sqrt{s}}{2} \int H_{ab}(x_a, x_b) \frac{1}{E_1} \frac{D_{H/c}(z_3)}{z_3} dz_3 dp_{T_2}^2 dy_2 \ . \tag{A-9}$$

The fractional longitudinal distribution of a pair of charmed hadrons, $x_{fp} = x_3 + x_4$, is

$$\frac{d\sigma}{dx_{fp}} = \int dx_3 dx_4 \delta(x_{fp} - x_3 - x_4) \frac{d\sigma}{dx_3 dx_4} \ . \tag{A-10}$$

Appendix B

Here we give the model forms for the intrinsic charm distributions that have been used in our calculations. We first give the intrinsic c quark momentum distributions and how they change due to fragmentation into charmed hadrons. We then give the charmed hadron distributions arising from recombination of intrinsic charmed quarks with the projectile valence quarks that produce a leading charm effect. Lastly, we give the distribution of $D\overline{D}$ pairs produced through fragmentation of both intrinsic heavy quarks as well as through a combination of fragmentation and recombination.

The intrinsic charm differential cross section for the n–particle Fock state is written as

$$\frac{d\sigma_{\rm ic}}{dx_1 \ldots dx_n} = N_n \frac{\delta(1 - \sum_{i=1}^n x_i)}{(m_h^2 - \sum_{i=1}^n (\widehat{m}_i^2/x_i))^2} \ , \tag{B-1}$$

where $\widehat{m}_i = \sqrt{m_i^2 + \langle \vec{k}_{\perp i}^2 \rangle}$ is the average transverse mass of the ith particle and N_n is an overall normalization factor. Assuming $\langle \vec{k}_{\perp i}^2 \rangle$ is proportional to the square of the quark mass, we adopt the effective values $\widehat{m}_c = 1.8$ GeV and $\widehat{m}_q = 0.45$ GeV.

The intrinsic c–quark distribution in the proton may be written as

$$\frac{d\sigma_{\rm ic}}{dx_c} = N_5 \int_0^{1-x_c} dx_1 \int_0^{1-x_c-x_1} dx_2 \int_0^{1-x_c-x_1-x_2} dx_{\bar{c}} \left[m_p^2 - \widehat{m}_c^2 \left(\frac{1}{x_c} + \frac{1}{x_{\bar{c}}} \right) - \widehat{m}_q^2 \left(\frac{1}{x_1} + \frac{1}{x_2} + \frac{1}{1-x_1-x_2-x_c-x_{\bar{c}}} \right) \right]^{-2} . \quad \text{(B-2)}$$

In the pion, we have

$$\frac{d\sigma_{\rm ic}}{dx_c} = N_4 \int_0^{1-x_c} dx_1 \int_0^{1-x_c-x_1} dx_{\bar{c}} \left[m_\pi^2 - \widehat{m}_c^2 \left(\frac{1}{x_c} + \frac{1}{x_{\bar{c}}} \right) - \widehat{m}_q^2 \left(\frac{1}{x_1} + \frac{1}{1-x_1-x_c-x_{\bar{c}}} \right) \right]^{-2} . \quad \text{(B-3)}$$

When the intrinsically produced heavy quarks are allowed to fragment in the same way as those produced by parton fusion, the resulting charmed hadron distribution is written as

$$\frac{d\sigma_{\rm ic}}{dx_D} = \int dz_3 dx_c D_{D/c}(z_3) \frac{d\sigma_{\rm ic}}{dx_c} \delta(x_D - z_3 x_c) , \quad \text{(B-4)}$$

where $D_{D/c}(z)$ is the fragmentation function of a c quark into a D meson and $d\sigma_{\rm ic}/dx_c$ is the intrinsic c quark distribution given above. These distributions are shown in Fig. 3 for protons and pions with both fragmentation functions.

The x distribution of a Λ_c produced by recombination of an intrinsic c quark with the proton valence quarks may be written as

$$\frac{d\sigma_{\rm ic}}{dx_{\Lambda_c}} = \int \prod_{i=1}^{5} dx_i \frac{d\sigma_{\rm ic}}{dx_1 \ldots dx_c} \delta(x_{\Lambda_c} - x_1 - x_2 - x_c) , \quad \text{(B-5)}$$

where $i = 1, 2, 3$ correspond to the light valence quarks while $x_4 \equiv x_{\bar{c}}$ and $x_5 \equiv x_c$, the intrinsic charm states. After integrating over x_3 and x_c with the delta functions, we are left with

$$\frac{d\sigma_{\rm ic}}{dx_{\Lambda_c}} = N_5 \int_0^{x_{\Lambda_c}} dx_1 \int_0^{x_{\Lambda_c}-x_1} dx_2 \int_0^{1-x_{\Lambda_c}} dx_{\bar{c}} \left[m_p^2 - \widehat{m}_c^2 \left(\frac{1}{x_{\Lambda_c}-x_1-x_2} + \frac{1}{x_{\bar{c}}} \right) - \widehat{m}_q^2 \left(\frac{1}{x_1} + \frac{1}{x_2} + \frac{1}{1-x_{\Lambda_c}-x_{\bar{c}}} \right) \right]^{-2} . \quad \text{(B-6)}$$

The corresponding $\overline{D}$ distribution is found from

$$\frac{d\sigma_{\rm ic}}{dx_{\overline{D}}} = N_5 \int_0^{x_{\overline{D}}} dx_3 \int_0^{1-x_{\overline{D}}} dx_2 \int_0^{1-x_{\overline{D}}-x_2} dx_c \left[m_p^2 - \widehat{m}_c^2 \left(\frac{1}{x_{\overline{D}}-x_3} + \frac{1}{x_c} \right) - \widehat{m}_q^2 \left(\frac{1}{x_3} + \frac{1}{x_2} + \frac{1}{1-x_{\overline{D}}-x_2-x_c} \right) \right]^{-2} , \quad \text{(B-7)}$$

where the delta function specifying the Λ_c momentum fraction has been replaced by $\delta(x_{\overline{D}} - x_3 - x_{\bar{c}})$ in the integral of Eq. (B-5). We have chosen the $\bar{c}$ to combine with valence quark 3 because 1 and 2 have gone into the production of the Λ_c. Another combination of valence quarks could alternatively lead to $\Sigma_c\overline{D}$ production with the same distribution for the $\overline{D}$ and equivalent distributions for Λ_c and Σ_c. The amplitudes of the production cross sections are equal, $d\sigma_{\rm ic}/dx_{\overline{D}} = d\sigma_{\rm ic}/dx_{\Lambda_c}$, when $x_{\overline{D}} = 1 - x_{\Lambda_c}$ and both hadrons are produced by this mechanism. The leading D^- and D^0 distributions in a π^- are calculated from

$$\frac{d\sigma_{\rm ic}}{dx_{D^0}} = N_4 \int_0^{x_{D^0}} dx_2 \int_0^{1-x_{D^0}} dx_{\bar{c}} \left[m_\pi^2 - \widehat{m}_c^2 \left(\frac{1}{x_{D^0} - x_2} + \frac{1}{x_{\bar{c}}} \right) - \widehat{m}_q^2 \left(\frac{1}{x_2} + \frac{1}{1 - x_{D^0} - x_{\bar{c}}} \right) \right]^{-2} . \tag{B-8}$$

The x distributions resulting from valence quark recombination are shown in Fig. 4.

The x_f distribution of a $D\overline{D}$ arising from intrinsic heavy quark pairs may be calculated in two ways, assuming either that both heavy quarks undergo fragmentation or that the $\bar{c}$ quark recombines to form a $\overline{D}$ meson while the c quark fragments into a D. In the first case,

$$\frac{d\sigma_{\rm ic}}{dx_{fp}} = \int dz_3 dz_4 D_{D/c}(z_3) D_{\overline{D}/\bar{c}}(z_4) dx_1 \ldots dx_{\bar{c}} \frac{d\sigma_{\rm ic}}{dx_1 \ldots dx_{\bar{c}}} \times \delta(x_{fp} - z_3 x_c - z_4 x_{\bar{c}}) , \tag{B-9}$$

where $x_D = z_3 x_c$ and $x_{\overline{D}} = z_4 x_{\bar{c}}$. Integration over the delta functions gives, for protons,

$$\frac{d\sigma_{\rm ic}}{dx_{fp}} = N_5 \int dz_3 dz_4 \frac{D_{D/c}(z_3) D_{\overline{D}/\bar{c}}(z_4)}{|z_4 - z_3|} \int_{x_{fp}/z_3}^{x_{fp}/z_4} dx_f \int_0^{1-x_f} dx_1 \int_0^{1-x_f-x_1} dx_2 \left[m_p^2 - \widehat{m}_c^2 \left(\frac{|z_4 - z_3|}{|x_f z_4 - x_{fp}|} + \frac{|z_4 - z_3|}{|x_{fp} - z_3 x_f|} \right) - \widehat{m}_q^2 \left(\frac{1}{x_1} + \frac{1}{x_2} + \frac{1}{1 - x_1 - x_2 - x_f} \right) \right]^{-2} . \tag{B-10}$$

We make a change of variable so that $x_f = x_{fp}/z_3 + y x_{fp} |1/z_4 - 1/z_3|$ where $0 \le y \le 1$ and restrict the values of x_f so that $0 \le x_f \le 1$. A similar equation is easily derived for pions. When the intrinsic $\bar{c}$ quark in a proton recombines into a $\overline{D}$, the expression

$$\frac{d\sigma_{\rm ic}}{dx_{fp}} = \int dz_3 dx_{\overline{D}} D_{D/c}(z_3) dx_1 \ldots dx_{\bar{c}} \frac{d\sigma_{\rm ic}}{dx_1 \ldots dx_{\bar{c}}} \times \delta(x_{\overline{D}} - x_3 - x_{\bar{c}}) \delta(x_{fp} - z_3 x_c - x_{\overline{D}}) , \tag{B-11}$$

is obtained. More specifically

$$\frac{d\sigma_{\rm ic}}{dx_{fp}} = N_5 \int dz_3 D_{D/c}(z_3) \int_0^{x_{cu}} dx_c \int_0^{1-x_{fp}-x_c(1-z_3)} dx_2 \int_0^{x_{fp}-z_3 x_c} dx_3 \left[m_p^2 - \widehat{m}_c^2 \left(\frac{1}{x_c} + \frac{1}{x_{fp} - z_3 x_c - x_3} \right) - \widehat{m}_q^2 \left(\frac{1}{x_2} + \frac{1}{x_3} + \frac{1}{1 - x_2 - x_{fp} - x_c(1 - z_3)} \right) \right]^{-2} , \tag{B-12}$$

where x_{c_u} is defined as either $x_{c_{u1}} = x_{fp}/z_3$ or $x_{c_{u2}} = (1 - x_{fp})/(1 - z_3)$ depending on the relative size of x_{fp} and z_3. If both $x_{c_{u1}}$ and $x_{c_{u2}}$ are less than 1, we choose x_{c_u} to be the larger of the two. If one is less than unity and the other greater, x_{c_u} is chosen to be the smaller. If both are greater than unity, the integral is zero. The pair distributions are shown in Fig. 5.

Figure Captions

Fig 1. The production of charmed hadrons through the parton fusion (pf) mechanism as a function of x_f for 400 GeV pp collisions [47]. The solid curve shows the result using Peterson function fragmentation and the dashed curve using delta function fragmentation.

Fig 2. An example of an intrinsic component of the proton Fock state.

Fig 3. Illustration of the fragmentation of intrinsic heavy quarks, given by Eq. (12). (a) Intrinsic fragmentation of charm quarks in a proton to D mesons. The dashed curve is from delta function fragmentation, the solid shows Peterson fragmentation. (b) Same as above for a pion projectile.

Fig 4. Charmed hadron distributions resulting from recombination with valence quarks. (a) Λ_c distribution in a proton projectile, given by Eq. (13), (b) $\overline{D}$ distribution from a proton projectile, (c) D^0, D^- distribution in a pion projectile.

Fig 5. Distribution of $D\overline{D}$ pairs from intrinsic $c\bar{c}$ pairs in the proton. (a) Intrinsic fragmentation of both heavy quarks, Eq. (14). The dashed curve shows delta function fragmentation for both quarks and the solid curve, Peterson fragmentation. (b) $D\overline{D}$ pair production with intrinsic fragmentation and valence quark recombination, Eq. (15). The dashed curve shows D production via delta function fragmentation and the solid curve D production using the Peterson function.

Fig 6. Calculations of single particle $D/\overline{D}$ distributions in 360 GeV $\pi^- p$ interactions. (a) Peterson function fragmentation compared with the $D/\overline{D}$ distribution of Ref. [4]. The solid curve shows the parton fusion distribution alone, the dashed includes intrinsic fragmentation only while the dot–dashed curve includes D^0 and D^- production by valence quark recombination. (b) Same as in (a) except with delta function fragmentation. (c) Leading charm production (D^0, D^-). Both calculations include intrinsic fragmentation and recombination with delta function fragmentation in the dashed curve and Peterson function in the solid curve. (d) Nonleading charm production (D^+, $\overline{D}^0$) by intrinsic fragmentation only. The dashed curve is with delta function fragmentation, the solid gives the Peterson function result.

Fig 7. Calculations of single particle $D/\overline{D}$ distributions compared to the 400 GeV pp data of Ref. [47,52]. (a) Calculations using Peterson function fragmentation compared with the $D/\overline{D}$ distribution [47]. The solid curve shows the parton fusion result, the dashed curve is a calculation assuming all charmed mesons are produced by intrinsic fragmentation alone, and the dot–dashed curve assumes that 50% of the $\overline{D}$'s are produced by valence quark recombination. (b) Same as in (a) using delta function fragmentation. (c) Leading $\overline{D}$ distribution, including recombination, compared to $\overline{D}^0$ and D^- data of Ref. [52]. The solid curve uses Peterson function fragmentation while the dashed curve gives the result with delta function fragmentation. (d) Nonleading

D distribution calculated with intrinsic fragmentation only, compared to D^0, D^+ data [52]. The dashed curve is a calculation with delta function fragmentation, the solid uses the Peterson function.

Fig 8. Calculations of inclusive $D/\overline{D}$ distributions compared with 800 GeV pp data [53]. (a) Our results with Peterson function fragmentation are compared to $D/\overline{D}$ data. The solid curve shows the parton fusion result, the dashed curve is a calculation assuming all charmed mesons are produced by intrinsic fragmentation alone, and the dot–dashed curve assumes that 50% of the $\overline{D}$'s are produced by valence quark recombination. (b) Same as in (a) using delta function fragmentation.

Fig 9. Charmed hadron production in pp collisions at the ISR. (a) Λ_c production at $x_{\Lambda_c} > 0.5$ compared with the data of Ref. [12]. The solid curve is a calculation of Λ_c production with Peterson function fragmentation and includes valence quark recombination and intrinsic fragmentation. The dashed curve is the result from parton fusion alone with Peterson function fragmentation. (b) D^+, D^0 distributions from Ref. [54] compared with calculations including D production by intrinsic fragmentation with delta function and Peterson function fragmentation shown in the dashed and solid curves, respectively.

Fig 10. The ratio of $A_{\rm eff}/A$ as a function of x_f for tungsten compared to proton targets using a 250 GeV π^- beam. The solid curve shows the result integrated over all p_T while the dashed curve illustrates our model (see Eqs. (19), (20)) with $p_T > 2$ GeV.

Fig 11. Our calculations are compared with $D/\overline{D}$ data from π^-Cu interactions at 230 GeV. from Ref. [8]. (a) We show our calculations for $\pi^- p$ reactions at 230 GeV. The solid curve shows Peterson function results for parton fusion only while the dashed curve includes intrinsic charm with nonleading D production by intrinsic fragmentation and leading D production by intrinsic fragmentation and valence quark recombination. The dot–dashed and dotted curves show the same results for delta function fragmentation. (b) Our results are compared with data for π^-Cu interactions. Notations are as in (a). (c) Leading D results for π^-Cu interactions with delta function (dot–dashed curve) and Peterson function fragmentation (solid curve) and for $\pi^- p$ results with delta function (dotted) and Peterson (dashed) fragmentation. (d) Same calculations for nonleading D production. Both (c) and (d) are compared with π^-Cu data.

Fig 12. Calculation of $D^\pm$ distributions compared to data from 340 GeV $\pi^- A$ interactions [25]. (a) The combined $D/\overline{D}$ distribution is shown with delta function (dashed curve) and Peterson function fragmentation (solid curve). The same calculations are shown for leading D^- (b) and nonleading D^+ (c) production.

Fig 13. Calculation of $D^\pm$ distributions compared with data from 250 GeV $\pi^- A$ interactions [3,50]. (a) The combined $D/\overline{D}$ distribution is shown with delta function (dot–dashed curve) and Peterson function fragmentation (dashed curve). A calculation with parton fusion alone, using the Peterson function, is shown in the solid curve. We

show our fusion plus intrinsic charm calculations for leading D^- production in (b). The solid curve is the Peterson function result while the dashed curve is for delta function fragmentation. The same calculations are shown in (c) for nonleading D^+ production.

Fig 14. We show $\alpha(x_f)$ for $\pi^- A$ interactions at 300 GeV as calculated in our model. The dashed curve shows delta function fragmentation, the solid curve, the Peterson function. These results are compared to those for $D^\pm$ mesons produced by 250 GeV $\pi^- A$ interactions [3] and the effective α found by the WA78 beam dump experiment [23], indicated by the band with $\langle x_f \rangle = 0.31$.

Fig 15. Calculations of charmed pair production compared to 800 GeV proton–emulsion data [49], shown as a function of the fractional momentum of the pair, $x_{fp} = x_D + x_{\overline{D}}$. Results using Peterson function fragmentation are shown with (dotted curve) and without (solid curve) intrinsic charm. Similar results are given using delta function fragmentation (dot–dashed and dashed curve respectively).

Fig 16. Calculations of $\mu^\pm$ distributions from semi-leptonic decays of charmed hadrons at RHIC energies. The solid curves show results for pAu collisions while the dashed curves illustrate pp interactions at $\sqrt{s} = 200$ GeV. Peterson function fragmentation results for the μ^- and μ^+ distributions are given in (a) and (b) while the results with the delta function are shown in (c) and (d).

Fig 17. Predictions of B meson distributions from pp collisions at 800 GeV. We show $B/\overline{B}$ results in (a) for Peterson function fragmentation with parton fusion alone (solid curve) and including intrinsic beauty with valence quark recombination (dashed curve). (b) The same results are given for delta function fragmentation. (c) Leading B distributions, including valence quark recombination. The solid curve is with Peterson function fragmentation, the dashed uses the delta function. (d) Nonleading $\overline{B}$ production by intrinsic fragmentation alone. The dashed curve is the delta function result, the solid, the Peterson function.

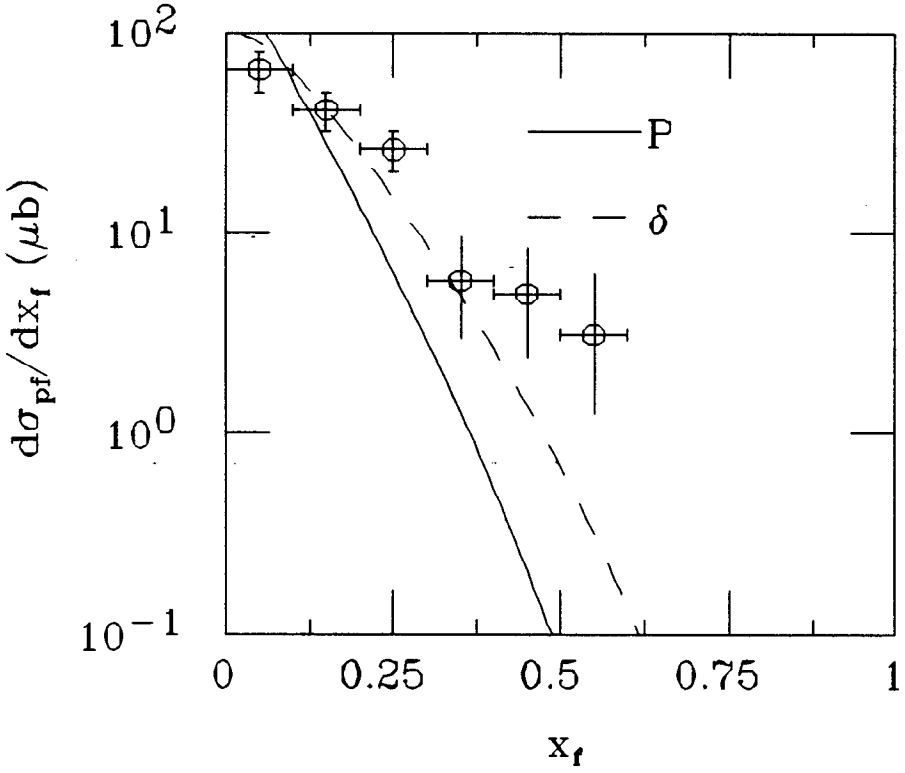

Fig. 1

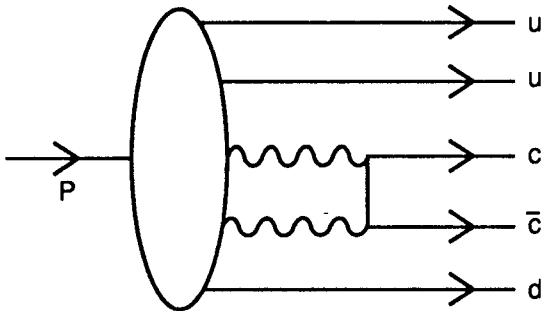

Fig. 2

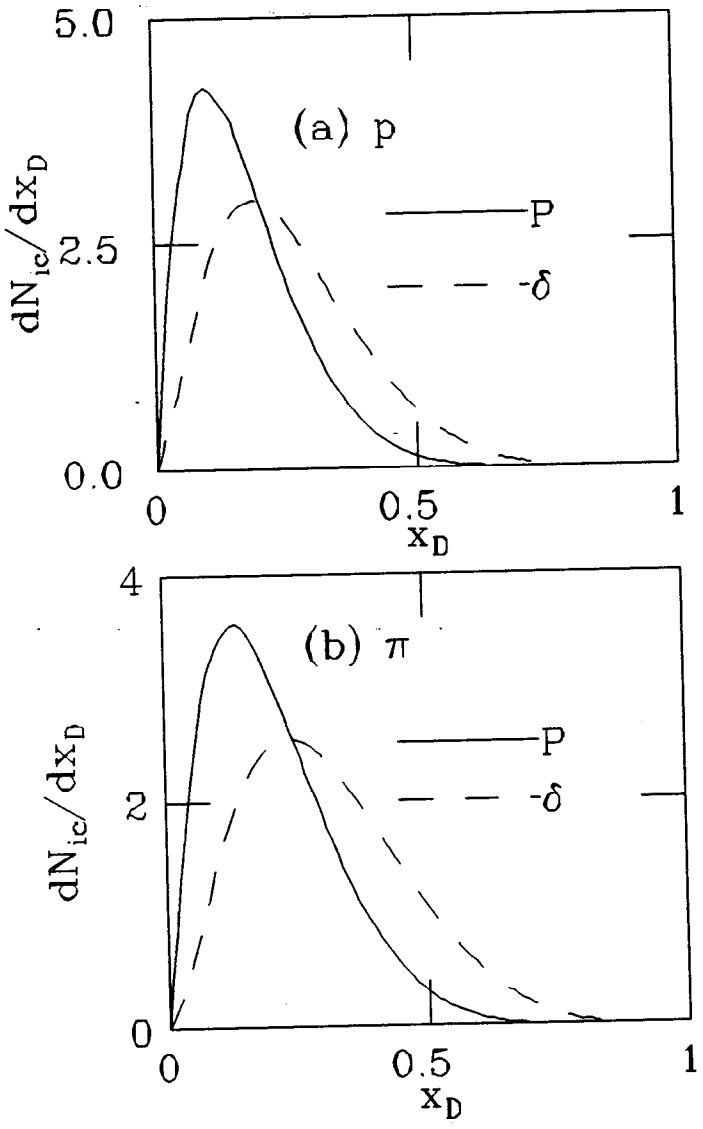

Fig. 3

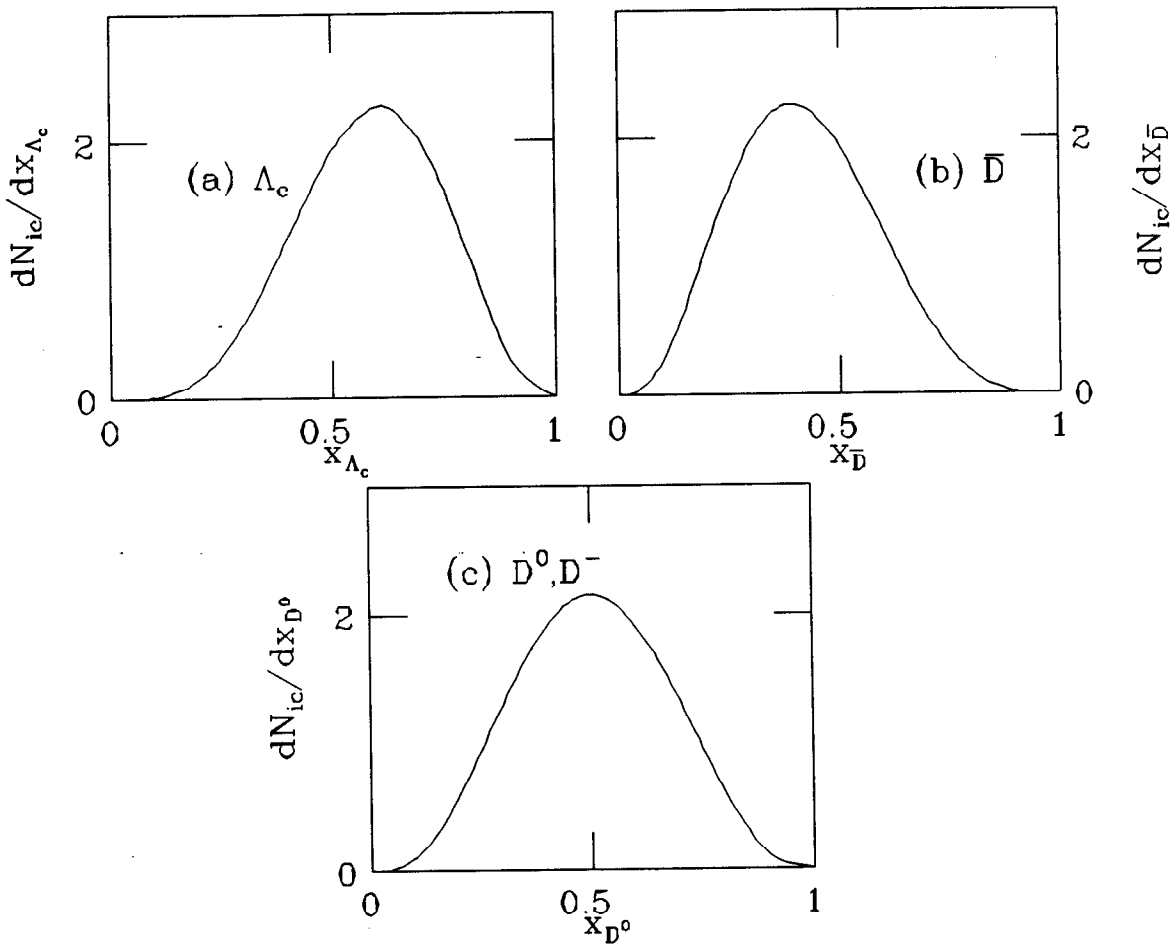
(a) Λ_c
(b) $\bar{D}$
(c) D^0, D^-
dN_{ic}/dx_{Λ_c}
$dN_{ic}/dx_{\bar{D}}$
dN_{ic}/dx_{D^0}
x_{Λ_c}
$x_{\bar{D}}$
x_{D^0}
0
0.5
1
2

Fig 4

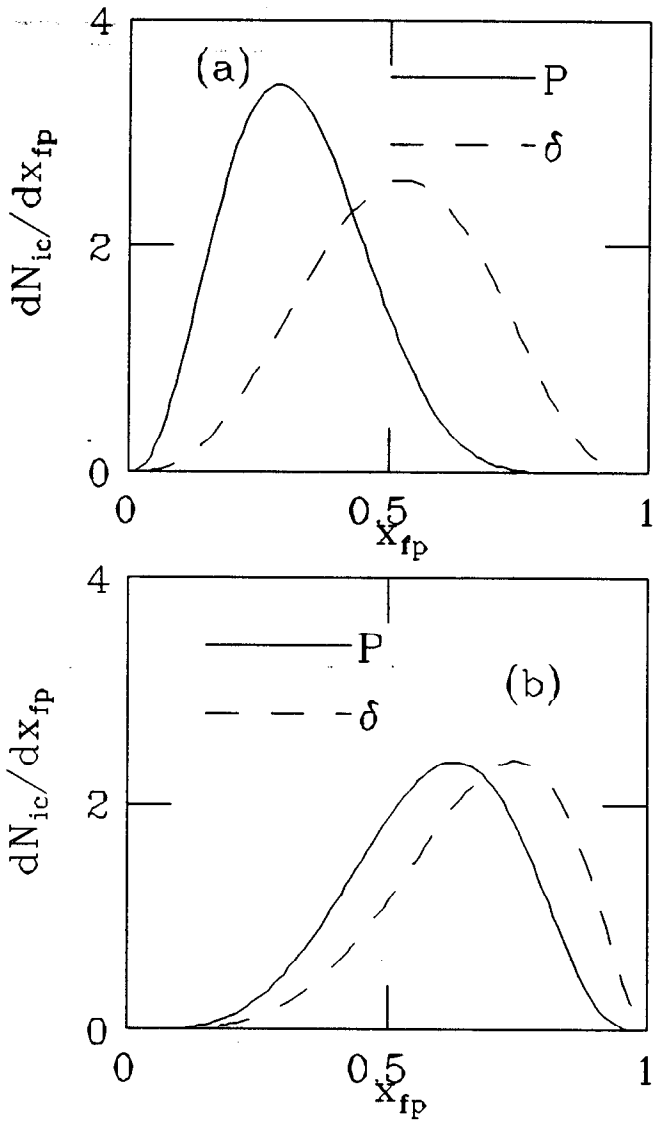

Fig. 5

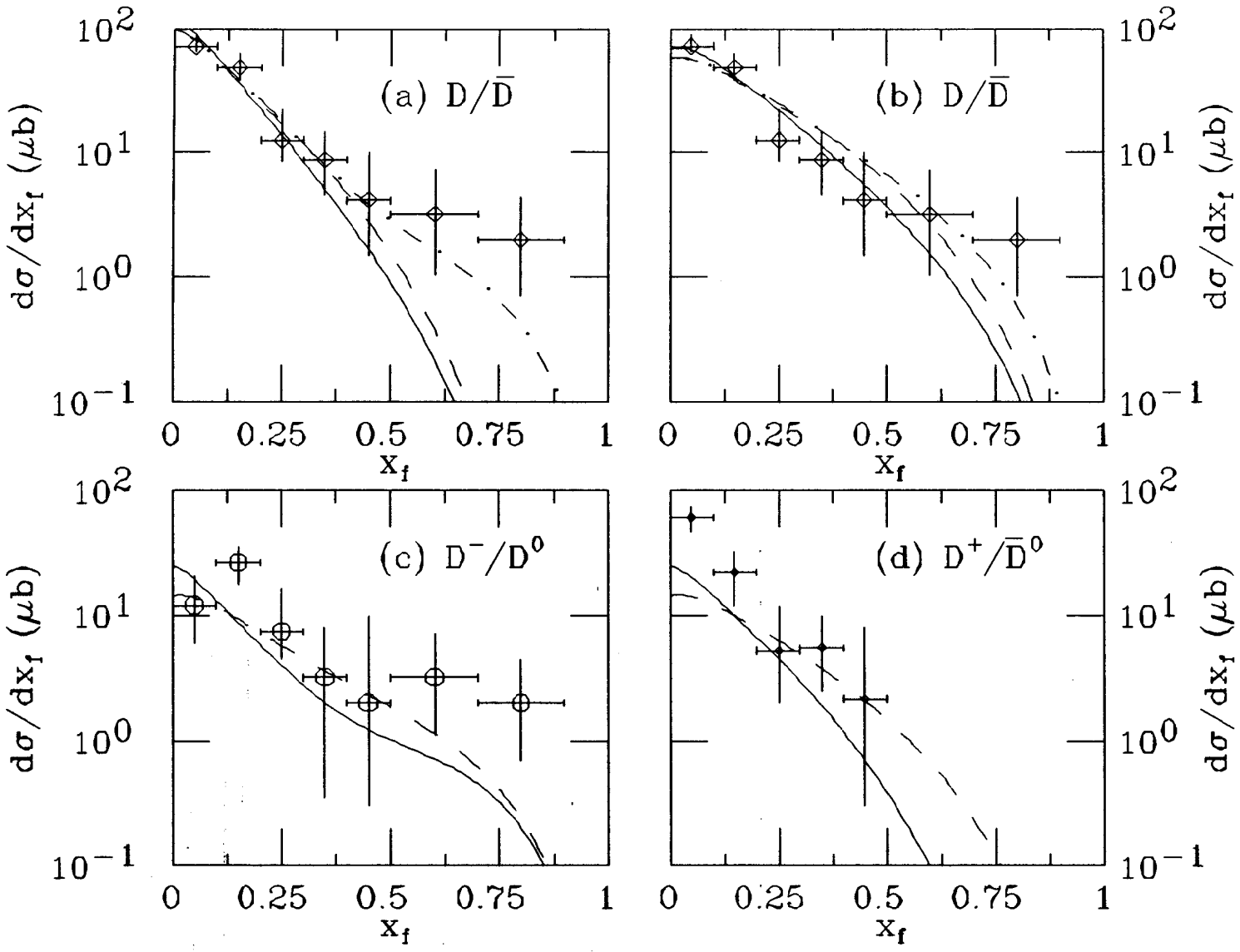

Fig. 6

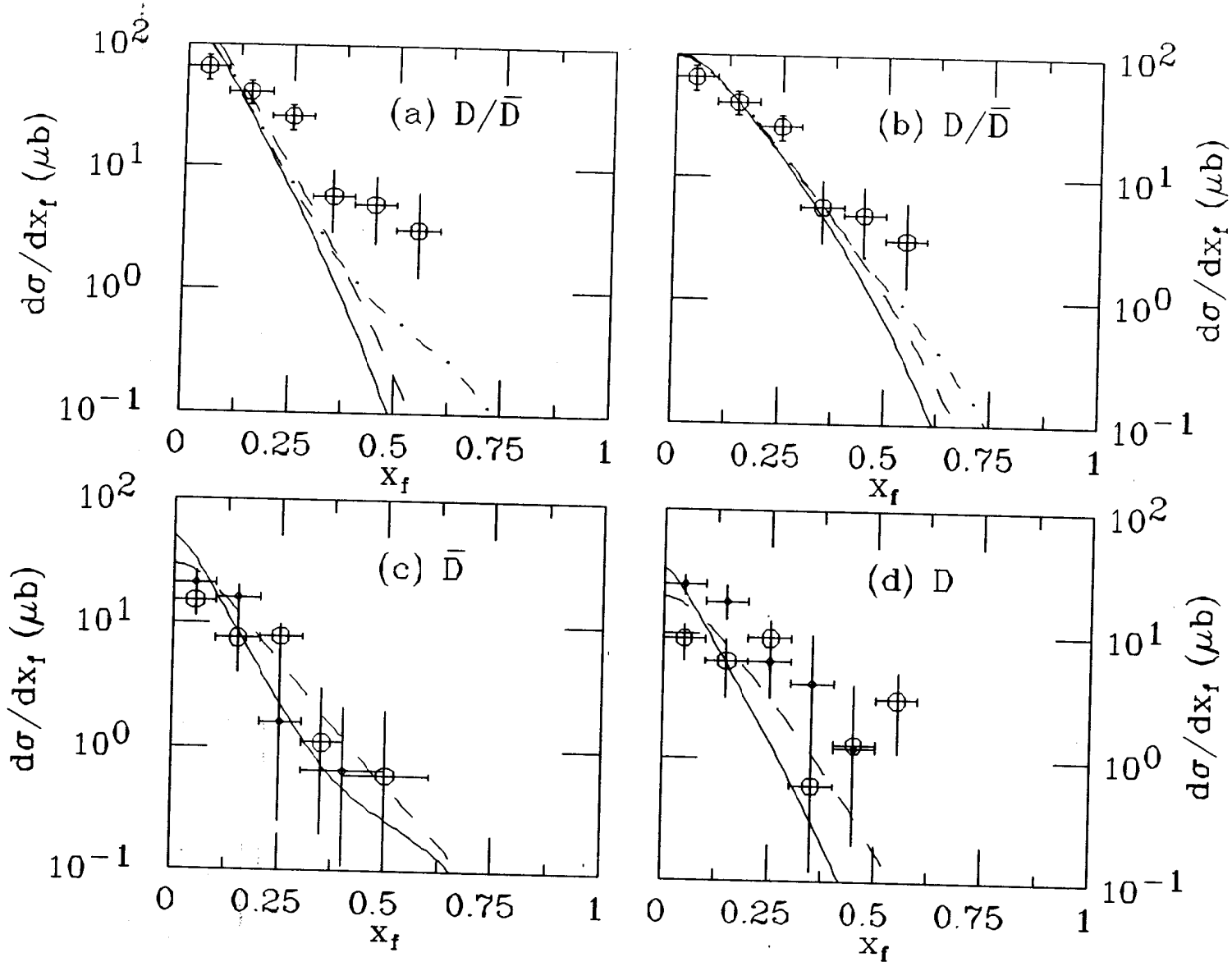
(a) D/$\bar{D}$
(b) D/$\bar{D}$
(c) $\bar{D}$
(d) D
$d\sigma/dx_f$ (μb)
x_f
10^2
10^1
10^0
10^{-1}
0
0.25
0.5
0.75
1

Fig. 7

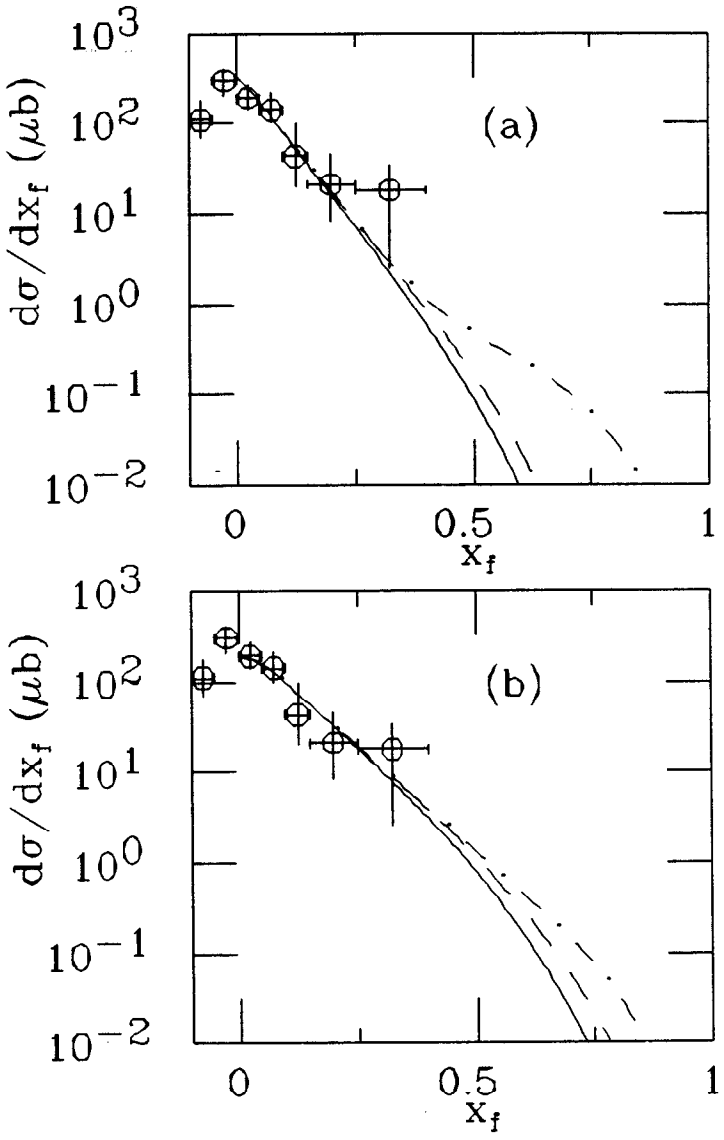
10^3
10^2
10^1
10^0
10^{-1}
10^{-2}
$d\sigma/dx_f$ (μb)
(a)
0
0.5
1
x_f
10^3
10^2
10^1
10^0
10^{-1}
10^{-2}
$d\sigma/dx_f$ (μb)
(b)
0
0.5
1
x_f

Fig. 8

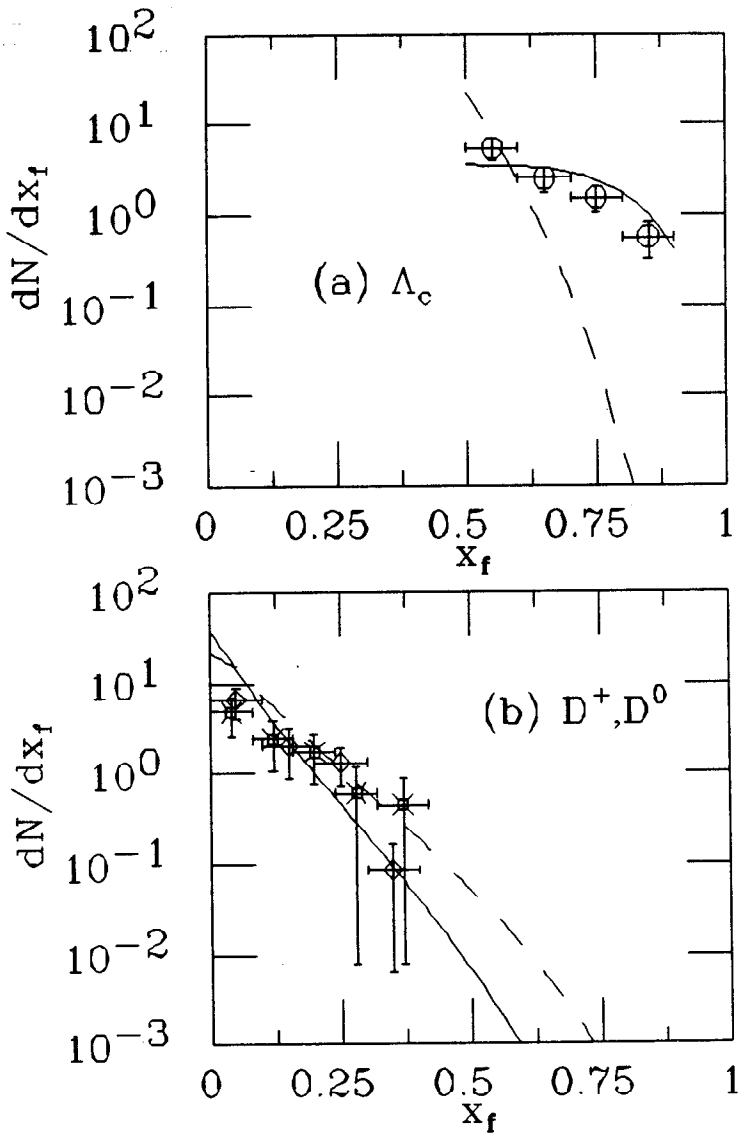
10^2
10^1
10^0
10^{-1}
10^{-2}
10^{-3}
dN/dx$_f$
(a) Λ_c
0
0.25
0.5
0.75
1
x$_f$
10^2
10^1
10^0
10^{-1}
10^{-2}
10^{-3}
dN/dx$_f$
(b) D^+,D^0
0
0.25
0.5
0.75
1
x$_f$

Fig. 9

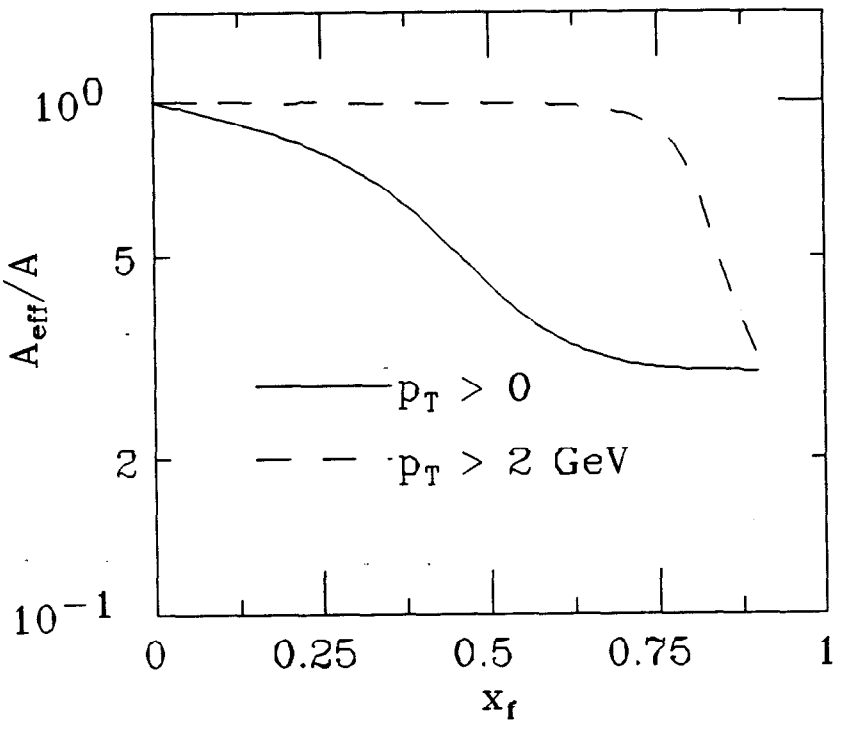

Fig. 10

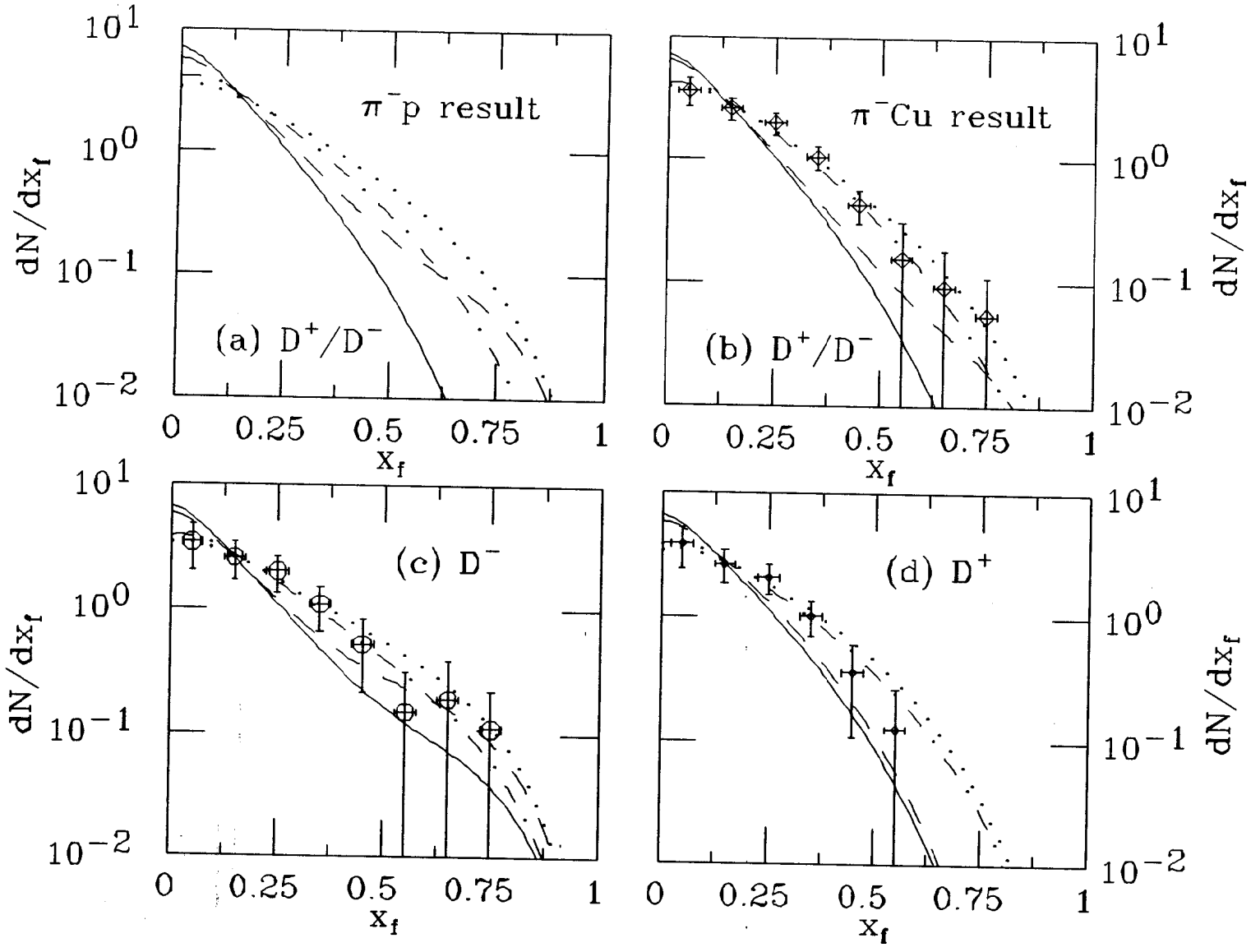
π^-p result
(a) D^+/D^-
π^-Cu result
(b) D^+/D^-
(c) D^-
(d) D^+
dN/dx_f
x_f
10^1
10^0
10^{-1}
10^{-2}
0
0.25
0.5
0.75
1

Fig. 11

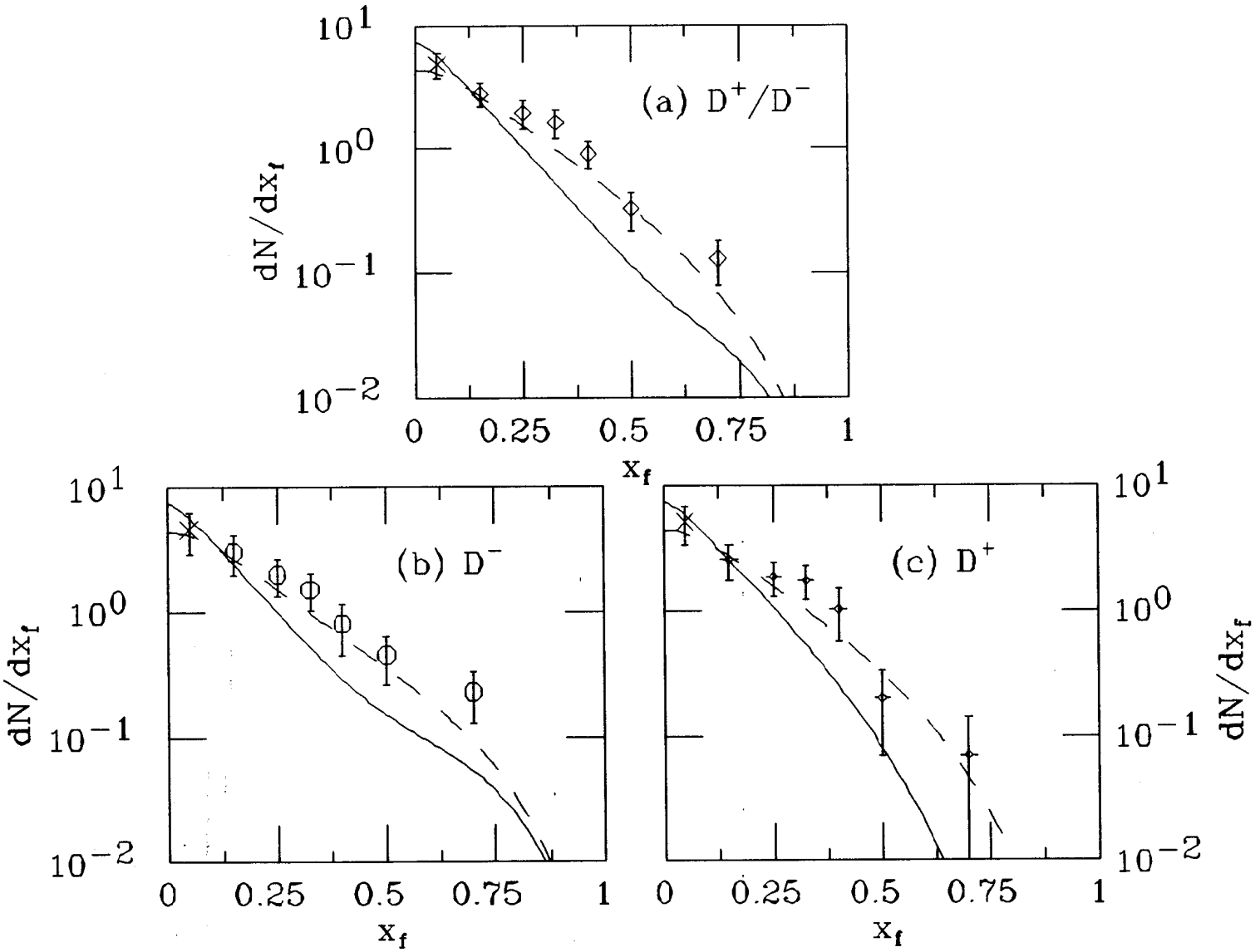

Fig. 12

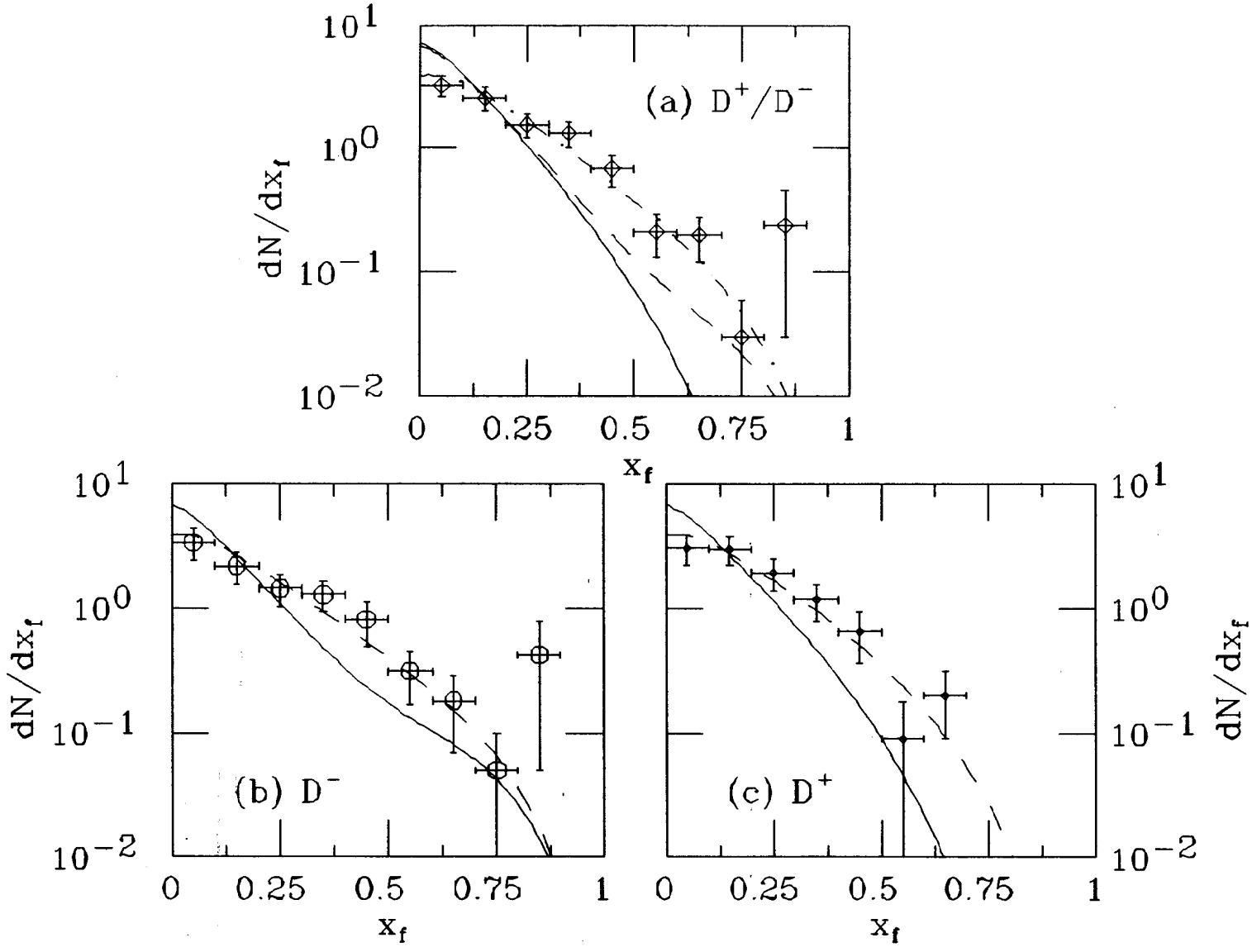

Fig. 13

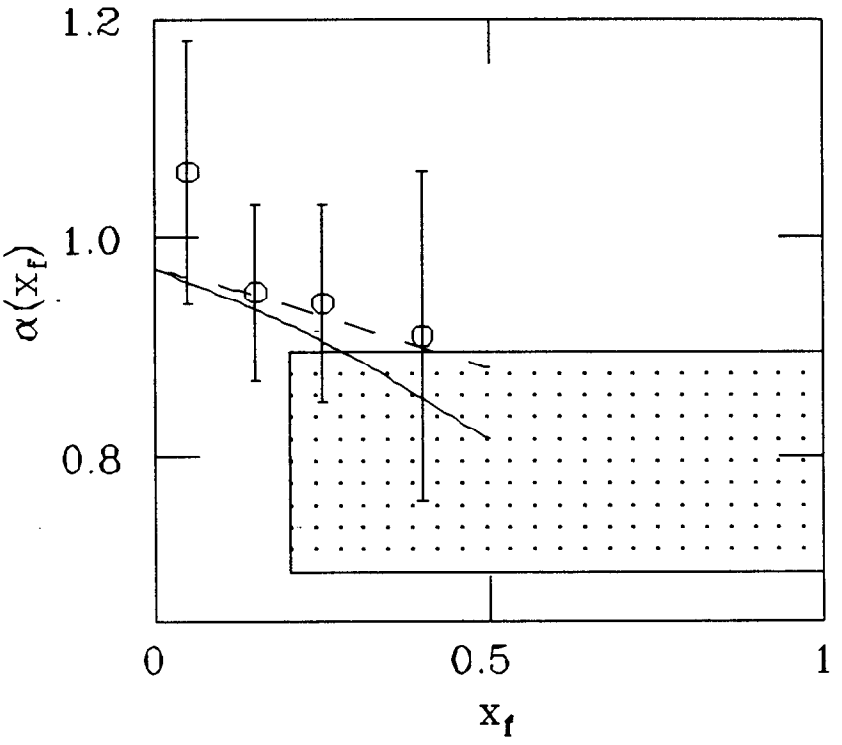

Fig. 14

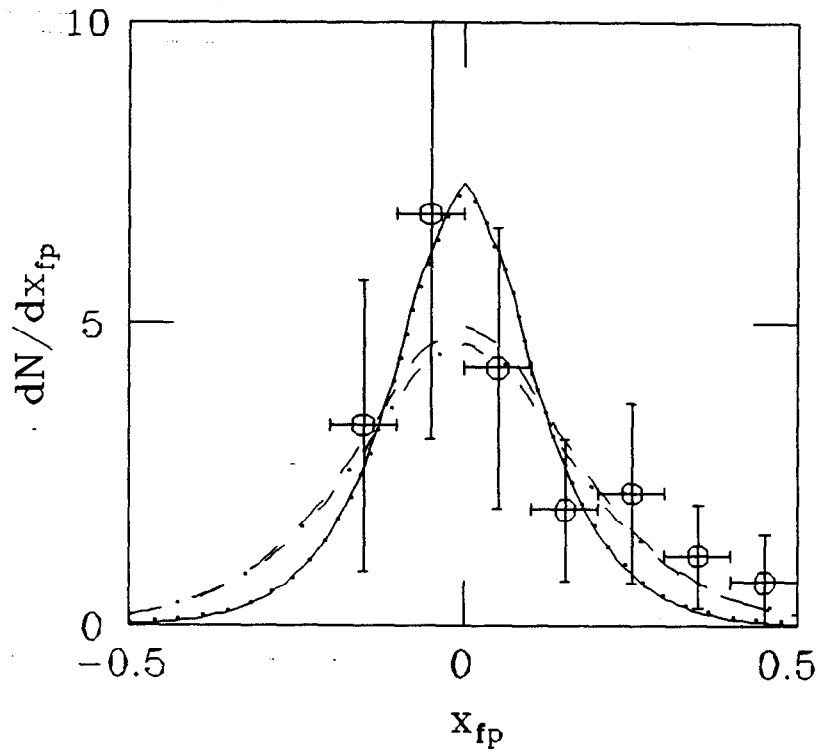

Fig. 15

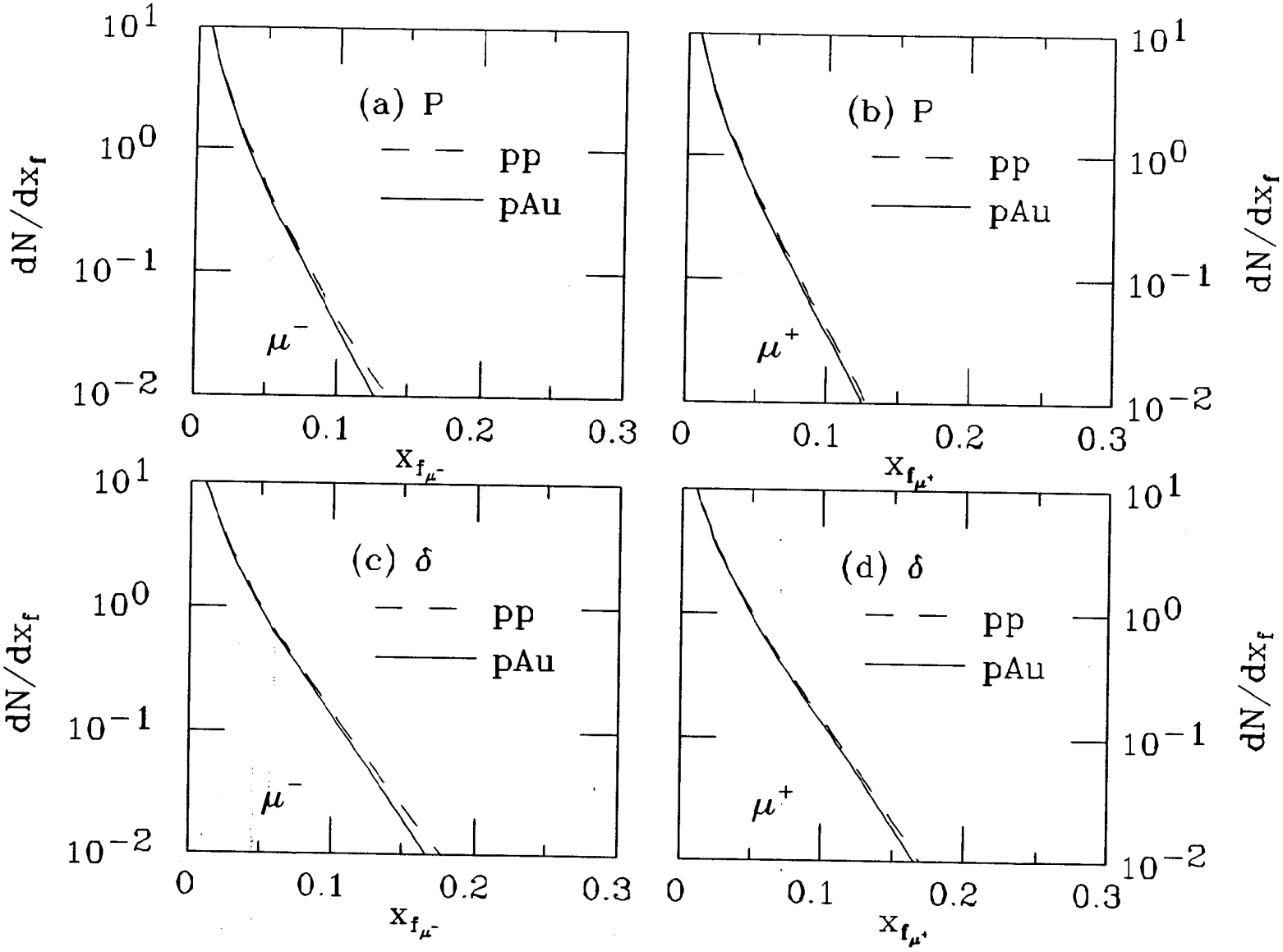
(a) P
pp
pAu
μ^-
(b) P
pp
pAu
μ^+
(c) δ
pp
pAu
μ^-
(d) δ
pp
pAu
μ^+
dN/dx_f
$x_{f_{\mu^-}}$
$x_{f_{\mu^+}}$
10^1
10^0
10^{-1}
10^{-2}
0
0.1
0.2
0.3

Fig. 16

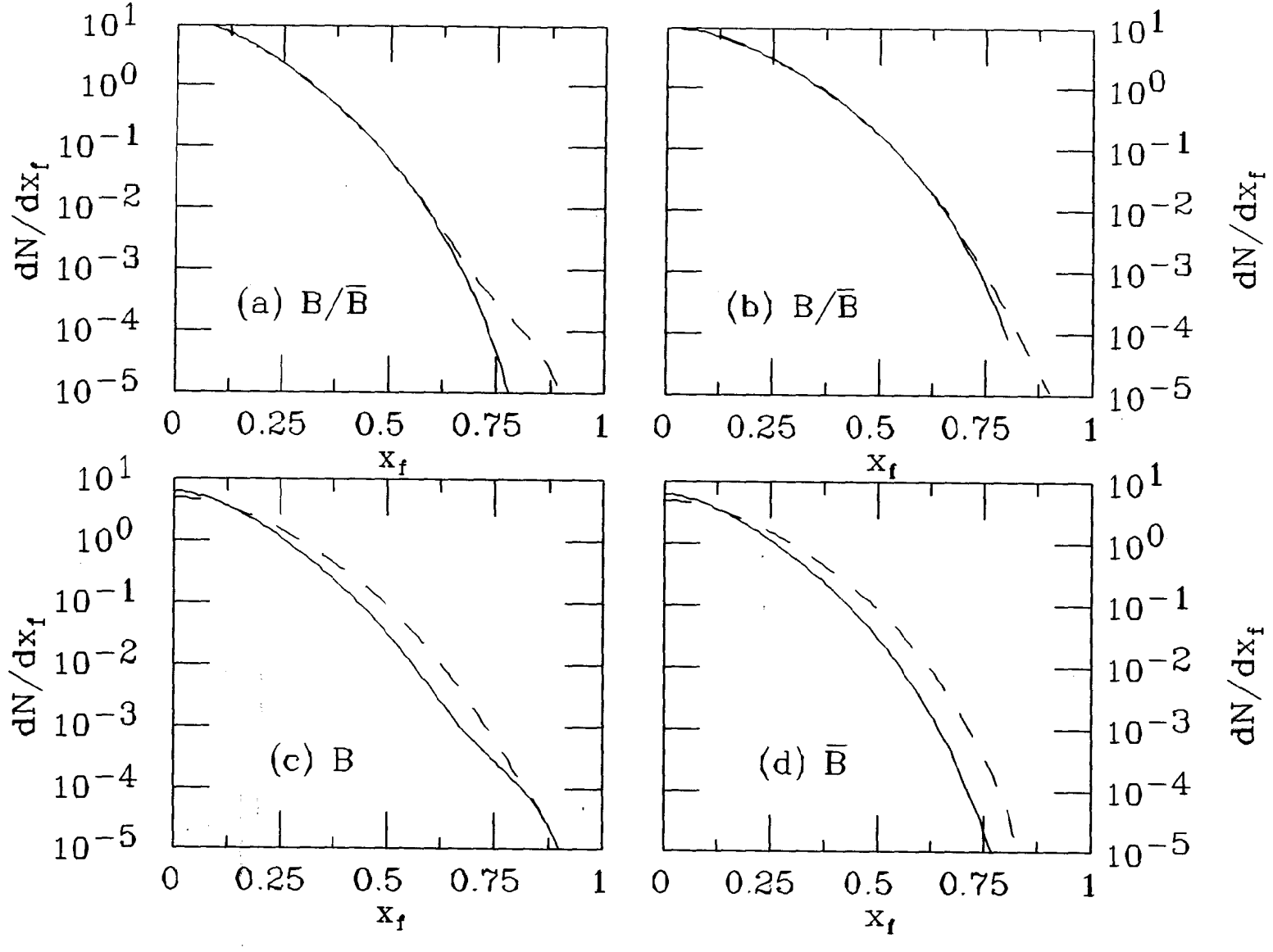
(a) B/$\bar{B}$
(b) B/$\bar{B}$
(c) B
(d) $\bar{B}$
dN/dx$_f$
x$_f$
0
0.25
0.5
0.75
1
10^1
10^0
10^{-1}
10^{-2}
10^{-3}
10^{-4}
10^{-5}

Fig. 17